UNIVERSITY OF CALIFORNIA SAN DIEGO

Boundary-Layer Analyses of Differential-Diffusion Effects In Laminar Jet Diffusion Flames

A thesis submitted in partial satisfaction of the
requirements for the degree
Master of Science

in

Engineering Science (Mechanical Engineering)

by

Akhil Nekkanti

Committee in charge:

Professor Antonio Sanchez, Chair
Professor Kalyanasundaram Seshadri
Professor Forman Williams

2018

The thesis of Akhil Nekkanti is approved, and it is acceptable in quality and form for publication on microfilm and electronically:

_____

_____

_____
Chair

University of California San Diego

2018

DEDICATION

To the scientific and research community for their relentless effort towards the progress of mankind.

EPIGRAPH

Anyone who has never made a mistake has never tried anything new.

—Albert Einstein

TABLE OF CONTENTS

LIST OF FIGURES

ACKNOWLEDGEMENTS

I owe my deepest gratitude to my advisor Professor Antonio Sanchez. I'm thankful to him for giving me opportunity to work in his group. I am extremely grateful for the valuable time he has spent in advising me. His continuous guidance, encouragement and support at all the levels of this work has enabled me to develop a better understanding of the subject and has helped me grow as a researcher.

I am also thankful to Dr. Wilfred Coenen, who's constant inputs have enhanced my skills in numerical modeling. His guidance and suggestions in programming have helped me a lot and I am grateful to him.

Last but not the least, I would also like to thank my parents who supported my decision to further my education.

VITA

2016	B. Tech. in Mechanical Engineering, Indian Institute of Technology, Ropar
2016-2017	Project Assistant, Indian Institute of Science, Bangalore
2017-2018	M. S. in Engineering Science (Mechanical Engineering), University of California San Diego

PUBLICATIONS

N Akhil, AL Sanchez, FA Williams, Explanations of influences of differential diffusion on flame-temperature variations in usual and inverse jet flames, (submitted) *Combustion and Flame*

RK Maurya, N Akhil. "Numerical investigation of ethanol fuelled HCCI engine using stochastic reactor model. Part 1: Development of a new reduced ethanol oxidation mechanism" . *Energy Conversion Management*. 118, 2016

RK Maurya, N Akhil. "Numerical investigation of ethanol fuelled HCCI engine using stochastic reactor model. Part 2: Parametric study of performance and emissions characteristics using new reduced ethanol oxidation mechanism." . *Energy Conversion Management*. 121, 2016

RK Maurya, N Akhil. "Development of a new reduced hydrogen combustion mechanism with NOx and parametric study of hydrogen HCCI combustion using stochastic reactor model" . *Energy Conversion Management*. 132, 2017

RK Maurya, N Akhil. "Comparative study of the simulation ability of various recent hydrogen combustion mechanisms in HCCI engines using stochastic reactor model". *International Journal Hydrogen Energy*. 42, 2017

ABSTRACT OF THE THESIS

Boundary-Layer Analyses of Differential-Diffusion Effects In Laminar Jet Diffusion Flames

by

Akhil Nekkanti

Master of Science in Engineering Science (Mechanical Engineering)

University of California, San Diego, 2018

Professor Antonio Sanchez, Chair

Theoretical and numerical studies of laminar jet diffusion flames have been conducted in the limit of infinitely fast chemistry for unity oxygen Lewis number $L_{\mathrm{O}} = 1$, providing information on flame shapes and flame temperatures for different reactant-feed dilution, fuel Lewis number L_{F}, and coflow-to-jet velocity ratios U_0. Shvab-Zel'dovich coupling functions are used to write the conservation equations for planar and axisymmetric jet flames in the boundary-layer approximation. Specific consideration is given to the mixing-layer solution near the injector rim, where differential-diffusion effects are seen to result in the expected superadiabatic/subadiabatic temperature for L_{F} smaller/larger than 1. These effects are more pronounced for $U_0 = 0$ and at intermediate values of Z_s. The

evolution of the temperature along the flame is found to exhibit an unexpected behavior, in that irrespective of the dilution and coflow velocity the flame temperature always transitions from superadiabatic to subadiabatic when $L_{\mathrm{F}} < 1$ and from subadiabatic to superadiabatic for $L_{\mathrm{F}} > 1$. The variation with L_{F} of the flame shape relative to the enthalpy field is reasoned as the cause for the observed transition. Additional computations are performed for inverse diffusion flames with $L_{\mathrm{O}} = 1$ and $L_{\mathrm{F}} \neq 1$. These do not exhibit reversed differential-diffusion behaviors, indicating that the diffusivity of the abundant (co-flow) reactant is less critical than that of the deficient (central-jet) reactant.

Chapter 1

Introduction

Combustion of gaseous fuels can be divided into premixed combustion and non-premixed combustion. In a premixed combustion the fuel and oxidizer are mixed before entering the reaction zone whereas in a non-premixed combustion the fuel and oxidizer are initially separated and are mixed in the same region where reaction is initiated. Diffusion plays a major role in the mixing of the fuel and oxidizer in non-premixed combustion and hence it is also called as diffusion combustion. Burning of a fuel jet in ambient air and candle flames are examples of diffusion flames. Applications of the diffusion flames include diesel engines, gas turbines, rocket engines and heating devices or domestic applications. This work deals with study of the flame shapes and flame temperatures of steady laminar jet diffusion flames.

The laminar jet diffusion flame has fuel flowing through the inner nozzle and air flowing through the outer annulus. The schematic of the laminar jet diffusion flame is given in Fig 1. In diffusion flames the combustion occurs at the interface between the fuel and air, where the burning of the fuel is controlled by the mixing process. The chemical reaction rate is generally much faster than the diffusion rates of the gaseous reactants. Accordingly, Burke and Schumann (BS) [1] suggested a flame sheet model that uses the approximation that the chemical reaction is infinitely fast in the diffusion flame and the reaction zone is infinitesimally thin. The Burke and Schumann model was able to predict the flame shape and flame height with good accuracy. This model considers a boundary-layer approximation by neglecting the axial diffusion and radial convection,

which were addressed in a few studies by researchers [2] [3] [4] and had obtained more accurate results. However these approaches involve more parameters, larger computation power and become more complex to obtain conclusions. Due to this the boundary layer approach has been preferred and is more useful [5].

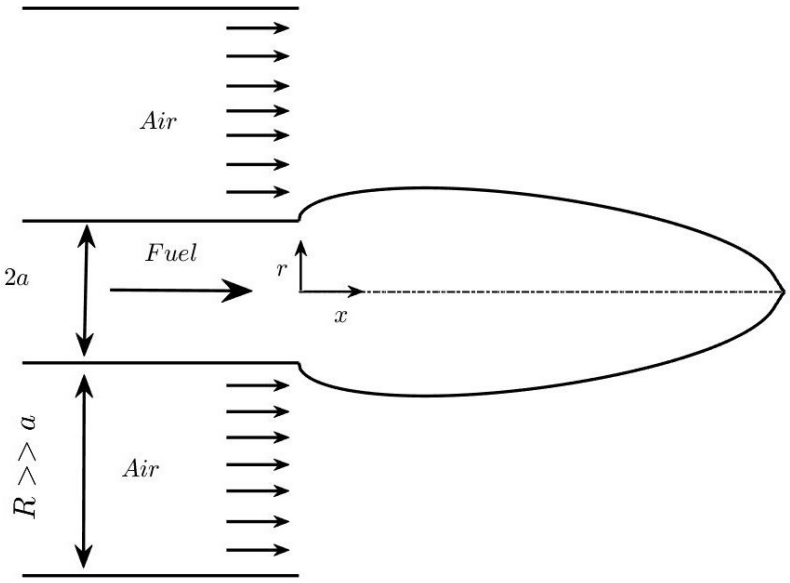

Figure 1: Schematic diagram of a coflowing laminar diffusion flame

Researchers have used several methods and approximations for solving the Navier-Stoke equations and the conservation equations for mixture fraction and enthalpy. Burke and Schumann (BS) [1] considered a one dimensional flow with axial velocity and constant density. Fay[6] have used a unity Prandtl number and unity Lewis number to simplify the system of equations, to solving only the equations of motion. They obtained that the flame temperature is the same as the adiabatic flame temperature. Klajan and Oppenheim [7] assumed unity Prandtl, Schmidt numbers and along with few assumptions were able to obtain an algebraic expression for flame height. Roper [8] had assumed an axial velocity that is independent of the radial coordinate and was able to find an approximate solution of the flame height for a unity Lewis and Schmidt number. With the assumption that the

fuel is injected as a point source researchers [9], [10] have obtained self similar solutions. Most of these works have neglected buoyancy effects while Roper[8] have treated in a simplified way. Many experimental studies have considered the gravity effects. Edelman et al. [11] have considered gravity effects with boundary-layer approximation and have obtained that in the presence of gravity the flames are much shorter in comparison to the zero gravity flames. Similar inferences were made by the experiments conducted by few other researchers in [12, 13, 14]. Sato et al. [15] obtained an empirical correlations of flame lengths with Reynolds number and Froude number. The work by Vazquez [5] focused in the limit of very low stoichiometric mixture fractions $Z_s \to 0$ and studied the effects of gravity and velocity of fuel and oxidizer stream. In this work it was reported that the flame lengths are inversely proportional to the level of gravity and a theoretical flame height was predicted that was in agreement with the experimental results. The results also showed that the flame length decreases as the coflow-to-jet velocity ratio increases. Li et al. [16] computed the flame heights in infinite atmosphere by considering the effects of buoyancy and by numerically integrating the boundary-layer equation with a suitable buoyancy scaling. They explored the effects of dilution and coflow velocities. They found that the flame heights were larger for larger fuel flow rates.

All these studies have used the approximation of a unity Lewis Number, which is a good approximation for the oxidizer that is air for most jet diffusion flames. However only methane and methanol exhibit a unity Lewis number, whereas most other fuels show a significant deviation from unity Lewis number. For a fuel with a unity Lewis number the Burke Schumann approximated flame temperature (T_f) is always equal to the adiabatic flame temperature (T_S) that is obtained by burning the fuel and oxidizer in stoichiometric proportions at a constant pressure [17]. For non unity Lewis numbers T_f vastly differs from T_S and the differential-diffusion effects result in superadiabatic flame temperatures for $L_{\mathrm{F}} < 1$ and subadiabatic flame temperatures for $L_{\mathrm{F}} > 1$ [18]. Though considerable work [19, 20, 21, 22, 23, 24, 25, 26] has been done for non unity Lewis numbers, the work involved the of finite-rate chemistry, only few literature [27, 28, 29] focuses on $L_{\mathrm{F}} \neq 1$ effects for Burke-Schumann type flames. The flame temperatures near the rim of the injector are found to be superadiabatic/subadiabaitic for L_{F} less than 1 / L_{F} greater than 1. Pitsch [30] attributed this to the differential-diffusion effects that are more prominent

near injector's rim. These effects have also been shown by Bergmann et al. [31]. Pitsch and Peters [32] have reported that the differential diffusion effects in hydrogen cause the flame to shift towards the leaner (oxidizer) side. Whereas for fuels with Lewis number greater than one the differential-diffusion effects shift the flame towards the fuel side. The effects of differential-diffusion and Lewis number are not so straight forward, hence this study is conducted to gain a better understanding of these effects in BS approximated laminar jet diffusion flames.

Diluted combustion is important in fire safety for fire extinction and is also useful in achieving higher fuel efficiency and lower emissions. Dilution is found to influence the flame lengths, Burke and Schumann [1] were the first to report shortened flame lengths in the case of fuel diluted with inert gases. Roper et al. [8] and Lee et al. [33] showed that dilution of fuel resulted in decreased flame lengths. Environment concerns and stringent emission regulations have led researcher to focus on methods to reduce soot and NO_x emissions. Researchers [34, 35, 36, 37, 38, 39, 40] observed that on diluting the fuel with N_2 resulted in lower soot formation. The reduction in soot was attributed to lowered fuel concentration and lowered flame temperature. Another important emission is the Nitrogen oxides (NO_x) it was observed by researchers [41, 42, 43] that on increases the velocity of the air stream the emission of (NO_x) decreases drastically for hydrogen jets. Chen and Driscoll [41, 42] have shown that the emission index of NO_x varies with the cube of the flame length and as the flame length decreases for larger coflow velocities of air, the emission of (NO_x) also decreases. The effect of coflow velocity on flame length was shown by Dahm [44], who reported that larger coflow velocity would reduce the amount of entertainment air required to dilute the fuel to stoichiometric proportions. In order to get a better understanding of these effects, the flame shapes and flame temperatures for different dilution and coflow velocities are analyzed.

Inverse diffusion flames (IDF) are similar to normal diffusion flames with the only difference that the position of fuel and oxidizer are interchanged. IDF configuration also play an important role in fire safety and space stations. The leaking of a oxygen jet caused an accidental fire which threatened the lives of the crew members on the Mir space station [45]. Researchers [46, 47, 48] have studied inverse diffusion flames as it would provide greater insight of the soot process. Sidebottoem and Glassman [46] reported that the

soot oxidation was absent in IDF and as a result the study of the soot formation would be easier. The flame shape is an important characteristic in inverse diffusion flame and has been studied by the researchers [47, 49, 50, 51]. Experiments done by Mikosfski et al. [49] showed that flame heights increase as the air flow rate increase and increase as dilution increases. However not much literature [46, 52] is available on the flame temperatures in IDF. In this study the flame shapes and flame temperatures for different dilutions and Lewis number in IDF are analyzed.

The primary objectives of this study is to increase understanding and provide accurate quantification of the effects of Lewis number, dilution, and coflow velocities on flame shapes and flame temperatures in BS laminar jet flames including both normal (fuel jet surrounded by oxidizer) and inverse (an oxidizer jet surrounded by fuel) configurations.

Chapter 2

Problem Formulation

Diffusion flames are flames in non-premixed combustion systems. We consider a co-flow burner in which the fuel and the air are provided by different gaseous feed streams, with dilution by addition of an inert gas permitted in the fuel-feed stream for generality. The subscripts F and A will be used to denote properties in the fuel and air streams, respectively for example, U_A and U_F are the velocities in the air and fuel feed streams while $Y_{\mathrm{O_2A}} = 0.232$ and $Y_{\mathrm{F_0}} \leq 1$ are the corresponding reactant mass fractions. The following chemical reaction is used in modeling the non-premixed combustion.

$$\mathrm{C_nH_{2n+2}} + \frac{3\mathrm{n}+1}{2}\mathrm{O_2} \rightarrow \mathrm{nCO_2} + (\mathrm{n}+1)\mathrm{H_2O} \tag{2.1}$$

For hydrogen ($n = 0$) the chemical reaction is as follows

$$2\mathrm{H_2} + \mathrm{O_2} \rightarrow 2\mathrm{H_2O} \tag{2.2}$$

The reactions 2.1, 2.2 are stoichiometric equations for the oxidation of a saturated hydrocarbon and hydrogen respectively. This chemical reaction implies that unit mass of fuel reacts with s=$8(3\mathrm{n}+1)/(7\mathrm{n}+1)$ units of $\mathrm{O_2}$ to produce $(22\mathrm{n})/(7\mathrm{n}+1)$ units of $\mathrm{CO_2}$ and $9(\mathrm{n}+1)/(7\mathrm{n}+1)$ units of $\mathrm{H_2O}$. s is defined as the mass of oxygen required to completely oxidize the fuel. The mass fraction of oxygen and fuel in the respective streams are denoted by $Y_{\mathrm{O_2A}} = 0.232$ and $Y_{\mathrm{F_0}}$. In a fuel-feed dilution the mass fraction of the fuel is less than 1 ($Y_{\mathrm{F_0}} \leq 1$.) The energy released is given by q=$\frac{1}{2}$ ($h^o_{\mathrm{C_nH_{2n+2}}}$-$h^o_{\mathrm{CO_2}}$-(n+1)$h^o_{\mathrm{H_2O}}$)/(7n+1). The mass of air required to oxidize a unit mass of the gaseous fuel stream to produce a

stoichiometric mixture is given by $S{=}sY_{\mathrm{F_0}}/Y_{\mathrm{O_{2A}}}$. Adiabatic combustion of the resulting mixture at constant pressure would produce a final temperature T_s, given by

$$T_s - T_A = \frac{T_F - T_A}{S+1} + \frac{qY_{F0}}{c_p(S+1)} \tag{2.3}$$

where T_A and T_F denote the temperatures of air and fuel streams respectively. The two parameters play a major role in non-premixed combustion are

$$S = \frac{sY_{\mathrm{F_0}}}{Y_{\mathrm{O_{2A}}}} \quad \text{and} \quad \gamma = \frac{qY_{F0}}{c_pT_A(S+1)} \tag{2.4}$$

Typical values for S and γ in a hydrocarbon-air flame with undiluted fuel feed (i.e., $Y_{\mathrm{F_0}} = 1$) initially at normal ambient temperature are $S_u = s/Y_{\mathrm{O_{2A}}} \approx 15$ and $\gamma \approx 6.5$, the latter corresponding to a peak temperature, $T_S \approx 2{,}300$ K.

In non-premixed combustion the fuel and oxidizer are mixed by diffusion and is the major factor in determining the burning rate. In diffusion flame the chemical reaction rate is much faster than the diffusion of the reactants and as a result of this the chemical reaction occurs in a narrow zone near the interface of the fuel and air. The reaction rate can be defined using the Arrhenius rate

$$\omega = Be^{-\frac{E}{RT}}\frac{\rho Y_F}{M_F}\frac{\rho Y_{O_2}}{M_{O_2}} \tag{2.5}$$

where $\rho Y_F/M_F$ and $\rho Y_{\mathrm{O_2}}/M_{\mathrm{O_2}}$ are the molar concentrations of the fuel and oxidizer respectively. Y is the mass fraction of the gas, ρ is the density of the gas, M is the molecular mass, R is the universal gas constant, E is the activation energy and B is the pre-exponential factor. B and E can be selected to reproduce the combustion characteristics of a given hydrocarbon [53].

The Navier-Stokes (NS) equations of mass, momentum, and energy along with conservation equations for the different chemical species [54] are used to describe the non-premixed combustion. The conservation species equations for the reaction (2.1) are

$$\frac{\partial}{\partial t}(\rho\hat{Y}_F) + \boldsymbol{\nabla}\cdot\left(\rho\mathbf{v}\hat{Y}_F - \frac{\rho D_T}{L_{\mathrm{F}}}\nabla\hat{Y}_F\right) = -\rho\hat{B}e^{-E/RT}\hat{Y}_F\hat{Y}_O \tag{2.6}$$

$$\frac{\partial}{\partial t}(\rho\hat{Y}_O) + \boldsymbol{\nabla}\cdot\left(\rho\mathbf{v}\hat{Y}_O - \rho D_T\nabla\hat{Y}_O\right) = S\rho\hat{B}e^{-E/RT}\hat{Y}_F\hat{Y}_O \tag{2.7}$$

$$\frac{\partial}{\partial t}(\rho\frac{T}{T_A}) + \boldsymbol{\nabla}\cdot\big(\rho\mathbf{v}\frac{T}{T_A} - \rho D_T\nabla\frac{T}{T_A}\big) = \gamma\big(1+S\big)\hat{B}e^{-E/RT}\hat{Y}_{\mathrm{F}}\hat{Y}_O - \frac{\boldsymbol{\nabla}\cdot\mathbf{q}_R}{c_pT_A} \qquad (2.8)$$

where the mass fractions are normalized using $\hat{Y}_F = Y_F/Y_{\mathrm{F}_0}$,$\hat{Y}_O = Y_O/Y_{\mathrm{O_{2A}}}$, the pre-exponential factor is normalized as $\hat{B} = \rho Y_{\mathrm{O_{2A}}}B/M_{\mathrm{O_2}}$. In the equations (2.6), (2.7) (2.8) $\mathbf{v}$ is the gas velocity D_T is the thermal diffusivity, L_{F} is the Lewis number of the fuel and $\boldsymbol{q}_R$ is the radiative heat flux. The initial and boundary conditions of the equation are $\hat{Y}_{\mathrm{F}} = 1$ $\hat{Y}_{\mathrm{O}} = 0$ and $T = T_{\mathrm{F}}$ in the fuel stream and $\hat{Y}_{\mathrm{F}} = 0$, $\hat{Y}_{\mathrm{O}} = 1$ and $T = T_{\mathrm{A}}$ in the air stream. For non-catalytic walls, the diffusion flux at the wall is zero $\mathbf{n}.\nabla\hat{Y}_{\mathrm{F}} = \mathbf{n}.\nabla\hat{Y}_{\mathrm{O}} = 0$. The boundary condition for temperature at the wall surface generally requires the solution of a conjugate heat conduction problem on the wall. The two limiting cases of practical use $T = T_w = constant$ for walls that are isothermal and $\mathbf{n}.\nabla T = 0$ for adiabatic walls.
In the above equation a few assumptions have been made. Firstly in the energy equation the specific heat is assumed to be a constant c_p by ignoring the variations due to change in temperature. Also it is assumed that the diffusion fluxes can be described by simple Fick's laws. Furthermore as N_2 is a major component of air, diffusivities of the reactants can be approximated by their binary diffusivities through N_2. This approximation is even more accurate for systems with N_2 dilution of the fuel stream. The diffusivity of oxygen is sufficiently close to D_T and the approximation $D_{\mathrm{O_2}} \approx D_T$ is used. Also the Lewis number of the oxidizer (i.e air) is approximately equal to 1 (L_O=1).

2.1 Burke-Schumann Approximation

In a diffusion flame the rate of the chemical reaction is much faster than the rate of diffusion of the reactants and due to this we assume that the Burke-Schumann limit is applicable. In the Burke-Schumann Limit [1], the reaction (2.1) is modeled as an infinitely fast reaction (i.e $B \to \infty$). The Burke-Schumann Limit has two important approximations. The first approximation is that the reaction zone is infinitesimally thin (Σ_f=0) at the interface between the fuel and oxygen and is considered as a flamelet. Secondly, the diffusion rate of fuel and oxidizer are in stoichiometric ratio at the flame surface and as a result the concentrations of the fuel and oxygen become zero at the flame

surface. The flame surface (Σ_f=0) separates a region of no fuel (i.e $\hat{Y}_{\rm F} = 0$ for $\Sigma > \Sigma_f$) and a region of no oxidizer (i.e $\hat{Y}_{\rm O} = 0$ for $\Sigma < \Sigma_f$). There is equilibrium on both sides of the flame sheet which implies that $\hat{Y}_F \hat{Y}_O = 0$ at the the flame sheet. The chemical species equations (2.6) and (2.7) can be combined using the Shvab-Zel'dovich coupling function [55, 56] along with the mixture fractions variables

$$Z = \frac{S\hat{Y}_{\rm F} - \hat{Y}_{\rm O} + 1}{S+1} \quad \text{and} \quad \tilde{Z} = \frac{S\hat{Y}_{\rm F}/L_{\rm F} - \hat{Y}_{\rm O} + 1}{S/L_{\rm F} + 1} \tag{2.9}$$

and the excess-enthalpy variable

$$\xi = \frac{c_p(T - T_A) + (q\hat{Y}_{\rm F_0}/S)(\hat{Y}_{\rm O} - 1)}{c_p(T_F - T_A) - q\hat{Y}_{\rm F_0}/S}, \tag{2.10}$$

which results in conservation equation

$$\frac{\partial}{\partial t}(\rho Z) + \nabla \cdot (\rho \mathbf{v} Z) - \frac{1}{L_m} \nabla \cdot \left(\rho D_{\rm T} \nabla \tilde{Z} \right) = 0, \tag{2.11}$$

$$\frac{\partial}{\partial t}(\rho \xi) + \nabla \cdot (\rho \mathbf{v} \xi) - \nabla \cdot (\rho D_{\rm T} \nabla \xi) = 0, \tag{2.12}$$

where $L_m = (S+1)/(S/L_{\rm F} + 1)$ and the boundary conditions are $Z = \tilde{Z} = \xi = 1$ in the fuel stream and $Z = \tilde{Z} = \xi = 0$ in the air stream. At the flame surface $\Sigma_f(\mathbf{x}, t) = 0$ the mass fractions of both the fuel and oxidizer are simultaneously zero $\hat{Y}_{\rm F} = \hat{Y}_{\rm O} = 0$, corresponding to values of the mixture fraction variables $Z = Z_s$ and $\tilde{Z} = \tilde{Z}_s$, with

$$Z_s = \frac{1}{S+1} \quad \text{and} \quad \tilde{Z}_s = \frac{1}{S/L_{\rm F} + 1}. \tag{2.13}$$

The equations (2.8) and (2.9) along with the chemical equilibrium condition $\hat{Y}_{\rm O}\hat{Y}_{\rm F} = 0$ gives the following relations for the mixture fraction and enthalpy variables.

$$\begin{cases} \hat{Y}_{\rm O} = 0, \ \hat{Y}_{\rm F} = \frac{Z - Z_s}{1 - Z_s} = \frac{\tilde{Z} - \tilde{Z}_s}{1 - \tilde{Z}_s} & \text{for } Z \geq Z_s \\ \hat{Y}_{\rm F} = 0, \ \hat{Y}_{\rm O} = 1 - \frac{Z}{Z_s} = 1 - \frac{\tilde{Z}}{\tilde{Z}_s} & \text{for } Z \leq Z_s \end{cases} \tag{2.14}$$

$$\begin{cases} \frac{T}{T_A} - 1 = \frac{T_F - T_A}{T_A}\xi + \frac{q}{S}(1 - \xi) & \text{for } Z \geq Z_s \\ \frac{T}{T_A} - 1 = \frac{T_F - T_A}{T_A}\xi + \frac{q}{S}(\frac{\tilde{Z}}{\tilde{Z}_s} - \xi) & \text{for } Z \leq Z_s \end{cases}, \tag{2.15}$$

the relation between T_F, T_S (adiabatic flame temperature), T_A and q/S, is given by

$$\frac{T_S - T_A}{T_A} = \frac{T_F - T_A}{T_A} Z_s + \frac{q}{S}(1 - Z_s) \tag{2.16}$$

The numerical solution is obtained by solving the equations (2.11) and (2.12) coupled with the Navier-Stoke equations. In the integration, the relationships (2.14) and (2.15) are employed to evaluate the temperature and composition in terms of Z and ξ, with the equation of state used to compute the density. Additionally, expressions must be provided for the transport properties in terms of the temperature and composition. The distribution of $\xi_f(\mathbf{x}, t)$ on the flame surface $\Sigma_f(\mathbf{x}, t) = 0$, to be obtained as part of the solution, determines the flame temperature T_f according to

$$\frac{T_f - T_A}{T_A} = \frac{T_F - T_A}{T_A}\xi_f + \frac{q}{S}(1 - \xi_f). \tag{2.17}$$

The solution simplifies greatly for $L_F = 1$, when $Z = \tilde{Z} = \xi$ everywhere in the flow field. Consequently, the flame value of ξ is simply $\xi_f = Z_s = 1/(S + 1)$ and the associated flame temperature evaluated from (2.17) becomes $T_f = T_S$, equal to the adiabatic flame temperature that is defined in (2.16). However, when $L_F \neq 1$, ξ_f differs from Z_s and as a result the flame temperature determined from equation (2.17) deviates from the stoichiometric adiabatic value by an amount given by

$$\frac{T_f - T_S}{(q/S)T_A + (T_A - T_F)} = Z_s - \xi_f, \tag{2.18}$$

As can be inferred from (2.18), since the characteristic temperature increase due to combustion $(q/S)T_A$ is much larger than $T_A - T_F$ for cases of practical interest, values of ξ_f higher/lower than Z_s correspond to subadiabatic/superadiabatic flame temperatures, respectively.

2.2 Steady Laminar Jet Diffusion Flames

In a jet flame, the radial (or transverse for a planar configuration) pressure gradient is negligible and only the axial momentum equation needs to be considered. Also the axial velocity and length are much larger than the radial velocity and length and as a result the axial diffusion can be neglected and this leads to a boundary-layer type equations. The governing equations for laminar jet diffusion flames take the following form

$$\frac{\partial}{\partial x}(\rho u) + \frac{1}{r^j}\frac{\partial}{\partial r}(r^j \rho v) = 0, \tag{2.19}$$

$$\rho u\frac{\partial u}{\partial x}+\rho v\frac{\partial u}{\partial r}=\frac{1}{r^j}\frac{\partial}{\partial r}(r^j\mu\frac{\partial u}{\partial r}) \tag{2.20}$$

$$\rho u\frac{\partial Z}{\partial x}+\rho v\frac{\partial Z}{\partial r}=\frac{1}{L_m}\frac{1}{r^j}\frac{\partial}{\partial r}(r^j\rho D_T\frac{\partial \tilde{Z}}{\partial r}) \tag{2.21}$$

$$\rho u\frac{\partial \xi}{\partial x}+\rho v\frac{\partial \xi}{\partial r}=\frac{1}{r^j}\frac{\partial}{\partial r}(r^j\rho D_T\frac{\partial \xi}{\partial r}) \tag{2.22}$$

where $j=0$ for planar geometry and $j=1$ for axisymmetric geometry.

The reactive mixture is assumed to behave as a ideal gas mixture with constant molecular mass. The thermal diffusivities are assumed to follow a power law of temperature. The spatial changes in pressure are small so that the equation of state reduces to

$$\rho T=\rho_A T_A,\quad \mu\sim(T)^\sigma\quad\text{and}\quad\frac{D_T}{D_{T_A}}=\Big(\frac{T}{T_A}\Big)^{\sigma+1} \tag{2.23}$$

It is shown in [57] that $\rho^2 D_T=$ constant and this implies that $\sigma=1$. The Howarth-Dorodnitsyn transformation is applied by introducing a density weighted transverse coordinate and a new transverse velocity

$$\big(\bar{r}\big)^{j+1}=(j+1)\int_0^r r^j\rho dr\quad\text{and}\quad\bar{v}=\Big(\frac{r}{\bar{r}}\Big)^j\Big(\rho v+\frac{u}{r^j}\frac{\partial}{\partial x}\int_0^r r^j\rho dr\Big) \tag{2.24}$$

For planar configuration the Howarth-Dorodnitsyn variable are given below

$$\bar{y}=\int_0^y\rho dy\quad\text{and}\quad\bar{v}=\Big(\rho v+u\frac{\partial}{\partial x}\int_0^y\rho dy\Big) \tag{2.25}$$

For axisymmetric configuration the Howarth-Dorodnitsyn variables are as follows

$$\bar{r}^2=\int_0^r 2\rho r dr\quad\text{and}\quad\bar{v}=\frac{r}{\bar{r}}\Big(\rho v+\frac{u}{r}\frac{\partial}{\partial x}\int_0^r\rho r dr\Big) \tag{2.26}$$

The equations (2.19),(2.20),(2.21),(2.22) are non-dimensionalized using the variables

$$\rho^*=\frac{\rho}{\rho_A},\quad U=\frac{u}{U_F},\quad r^*=\frac{\bar{r}}{a},\quad x^*=x\frac{D_T}{U_F a}\quad\text{and}\quad V=v\frac{a}{D_T} \tag{2.27}$$

Substituting the Howard-Dorodnitsyn and the non-dimensional variables (and removing the *) continuity, momentum, mixture fraction and enthalpy equations are simplified and take the form:

$$\frac{\partial U}{\partial x} + \frac{1}{r^j}\frac{\partial}{\partial r}(r^j V) = 0 \tag{2.28}$$

$$U\frac{\partial U}{\partial x} + V\frac{\partial U}{\partial r} = \frac{Pr}{r^j}\frac{\partial}{\partial r}(\Delta r^j \frac{\partial U}{\partial r}) \tag{2.29}$$

$$U\frac{\partial Z}{\partial x} + V\frac{\partial Z}{\partial r} = \frac{1}{L_m}\frac{1}{r^j}\frac{\partial}{\partial r}(\Delta r^j \frac{\partial \tilde{Z}}{\partial r}) \tag{2.30}$$

$$U\frac{\partial \xi}{\partial x} + V\frac{\partial \xi}{\partial r} = \frac{1}{r^j}\frac{\partial}{\partial r}(\Delta r^j \frac{\partial \xi}{\partial r}) \tag{2.31}$$

$$\Delta = \frac{2}{r^2}\int_0^r \frac{r'}{\rho} dr'$$

$\Delta = 1$ for a planar case. And for the axisymmetric case the approximation that $\Delta = 1$ is used for simplicity. The system of equations must be integrated along with the initial conditions

$$x = 0 \begin{cases} Z = \tilde{Z} = \xi = U = 1 & \text{for } r \leq 1 \\ Z = \tilde{Z} = \xi = 0,\ U = U_0 & \text{for } r \geq 1 \end{cases} \tag{2.32}$$

And the boundary conditions are

$$x > 0 \begin{cases} r = 0: \quad V = \frac{\partial U}{\partial r} = \frac{\partial Z}{\partial r} = \frac{\partial \tilde{Z}}{\partial r} = \frac{\partial \xi}{\partial r} = 0 \\ r = \infty: \quad Z = \tilde{Z} = \xi = 0, \quad U = U_0 \end{cases} \tag{2.33}$$

where $U_0 = U_A/U_F$. The flame sheet is determined by the location at which Z=Z_s or $\tilde{Z} = \tilde{Z}_s$. If the velocities of the fuel and air streams are equal i.e $U_0 = 1$ (as $U_A = U_F$) the system of equation simplify greatly to the following equations:

$$\frac{\partial Z}{\partial x} = \frac{1}{L_m}\frac{1}{r^j}\frac{\partial}{\partial r}(r^j \frac{\partial \tilde{Z}}{\partial r}) \tag{2.34}$$

$$\frac{\partial \xi}{\partial x} = \frac{1}{r^j}\frac{\partial}{\partial r}(r^j \frac{\partial \xi}{\partial r}) \tag{2.35}$$

The equations (2.34), (2.35) must be solved along with the following initial and boundary conditions

$$x = 0 \begin{cases} Z = \tilde{Z} = \xi = 1 & \text{for } r \leq 1 \\ Z = \tilde{Z} = \xi = 0, & \text{for } r \geq 1 \end{cases} \tag{2.36}$$

$$x > 0 \begin{cases} r = 0: & \frac{\partial Z}{\partial r} = \frac{\partial \tilde{Z}}{\partial r} = \frac{\partial \xi}{\partial r} = 0 \\ r = \infty: & Z = \tilde{Z} = \xi = 0 \end{cases} \tag{2.37}$$

2.3 Analytical Solution for Special Cases

Analytical solution is possible when the coflow velocities are the same i.e $U_0 = 1$ and the Lewis number of fuel is unity. $L_{\text{F}} = 1$ implies that $Z = \tilde{Z}$ and the system of equations reduces to the form

$$\frac{\partial Z}{\partial x} = \frac{1}{r^j}\frac{\partial}{\partial r}(r^j \frac{\partial Z}{\partial r}) \tag{2.38}$$

$$\frac{\partial \xi}{\partial x} = \frac{1}{r^j}\frac{\partial}{\partial r}(r^j \frac{\partial \xi}{\partial r}) \tag{2.39}$$

These parabolic equations must be solved along with the following initial and boundary conditions.

$$x = 0 \begin{cases} Z = \xi = 1 & \text{for } r \leq 1 \\ Z = \xi = 0, & \text{for } r \geq 1 \end{cases} \tag{2.40}$$

$$x > 0 \begin{cases} r = 0: & \frac{\partial Z}{\partial r} = \frac{\partial \xi}{\partial r} = 0 \\ r = \infty: & Z = \xi = 0 \end{cases} \tag{2.41}$$

In a planar case (j=0) introducing a self similar variable $\eta = (y-1)/\sqrt{2x}$ lead us to the following solution

$$Z = \xi = \frac{1}{2}\Big(\text{erf}\Big(\frac{1-y}{2x}\Big) + \text{erf}\Big(\frac{y+1}{2x}\Big)\Big) \tag{2.42}$$

In a axisymmetric case (j=1) the solution is given by the P - function [16, 51, 58].

$$Z = \xi = \frac{1}{2x}\exp\Big\{-\frac{r^2}{4x}\Big\}\int_0^1 \exp\Big\{-\frac{u^2}{4x}\Big\} I_0\Big(\frac{ur}{2x}\Big) u du \tag{2.43}$$

Where I_0 is zeroth order modified Bessel function of the first kind

2.4 Solution for $x << 1$

For small x, a self similar solution is possible and both the planar and axisymmetric configuration reduce to the same equation so in this section, y is used in place of r. $\partial U/\partial x \sim 1/x$ and $V \sim 1/\sqrt{x}$ and we introduce a self-similar variable $\eta = (y-1)/\sqrt{2x}$, a stream function ψ and a normalized stream function F such that $\psi = \sqrt{2x}F(\eta)$.

$$U = \frac{\partial \psi}{\partial y} = F'(\eta) \quad V = -\frac{\partial \psi}{\partial x} = \frac{1}{\sqrt{2x}}\big(\eta F'(\eta) - F(\eta)\big) \tag{2.44}$$

The equations for momentum, mixture fraction and enthalpy in self-similar variable are given below.

$$PrF''' + FF'' = 0 \tag{2.45}$$

$$\frac{1}{L_m}\tilde{Z}'' + FZ' = 0 \tag{2.46}$$

$$\xi'' + F\xi' = 0 \tag{2.47}$$

And the boundary conditions are

$$\begin{cases} \eta = -\infty : F' = Z = \tilde{Z} = \xi = 1, \quad (F-\eta)_{-\infty} \to 0 \\ \eta = \infty : \quad F'(\infty) - U_0 = Z = \tilde{Z} = \xi = 0 \end{cases} \tag{2.48}$$

At η_f, $Z = Z_s$ and the flame location $y_f = 1 + \eta_f\sqrt{2x}$

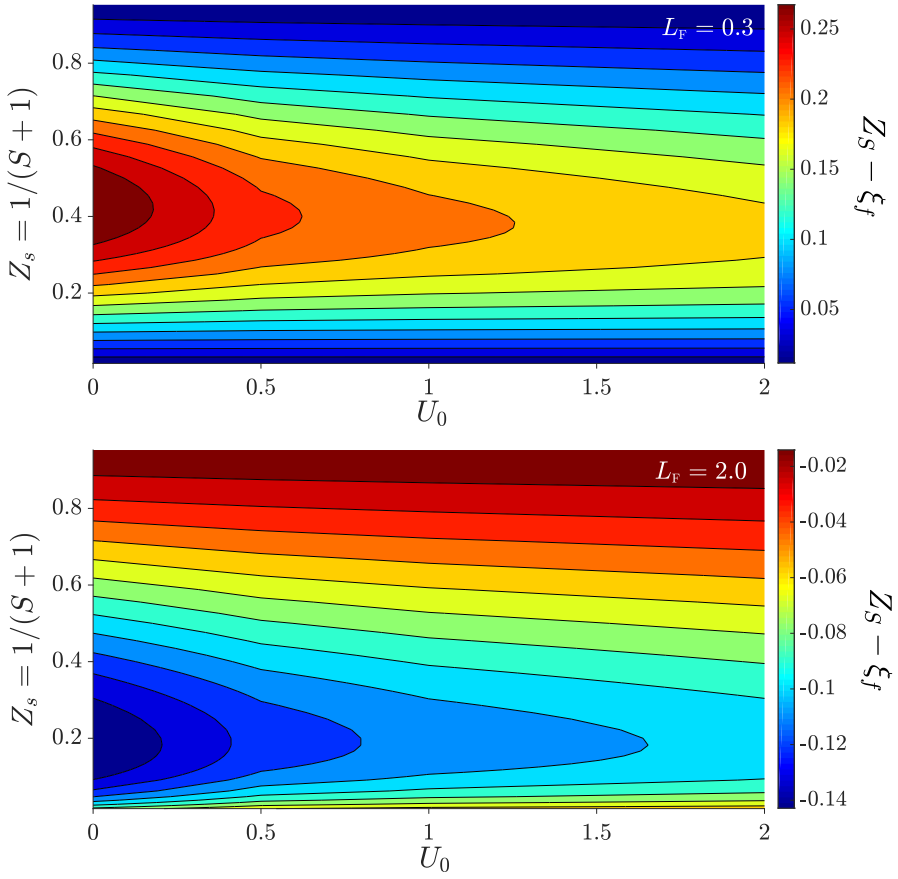

Figure 2: The contour plots showing the variation of dimensionless temperatures departures $Z_s - \xi_f$ as a function of $Z_s = 1/(S+1)$ and coflow velocity (U_0) for $L_F = 0.3$ (top) and for $L_F = 2.0$ (bottom)

The temperature departure $Z_s - \xi_f$ represents the nature of the flame temperature. Values of $Z_s - \xi_f$ at the injector rim ($x << 1$) are computed for different coflow velocities, dilutions and Lewis numbers and are presented in Fig. 2. The temperature departures near the injector rim give an indication of the differential diffusion-effects. Contour plot at the top conveys that the flame temperatures are superadiabatic ($Z_s - \xi_f > 0$) for $L_F = 0.3$, whereas subadiabatic flame temperatures ($Z_s - \xi_f < 0$) are observed for $L_F = 2.0$. For both the Lewis numbers, $|Z_s - \xi_f|$ start increasing from zero at $Z_s \to 0$ reach a maximum at an intermediate value of Z_s and then decrease. $L_F = 0.3$, exhibits a maximum temperature departure of $Z_s - \xi_f = 0.25$ at $Z_s = 0.4$. This indicates that the flame temperature is 25% times larger than the adiabatic temperature. Similarly for $L_F = 2.0$, $Z_s - \xi_f = -0.15$ is

observed at $Z_s = 0.2$, which implies that for a dilution of $S = 4$ the flame temperatures are subadiabatic by 15%. As the coflow velocity increases, for a particular dilution the $|Z_s - \xi_f|$ decreases, implying a lesser prominence of the differential-diffusion effects. It can be inferred from Fig. 2 that the differential-diffusion effects are more pronounced in stagnant air (U_0) for intermediate values of Z_s.

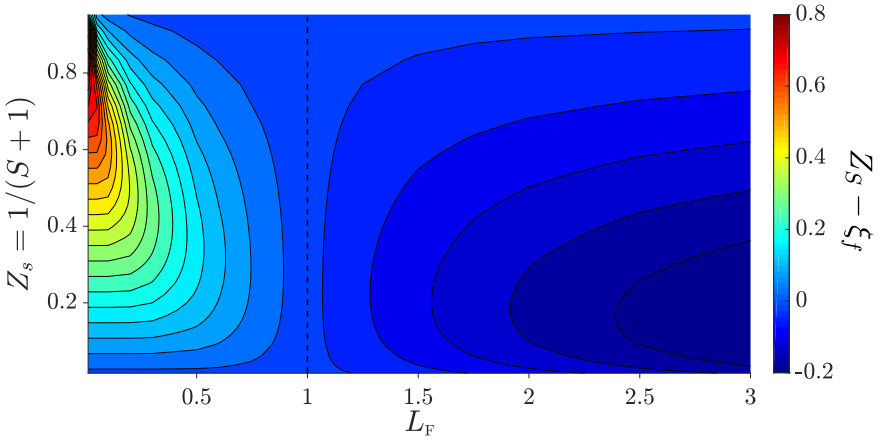

Figure 3: The contour plots showing the variation of dimensionless temperatures departures $Z_s - \xi_f$ as a function of $Z_s = 1/(S+1)$ and Lewis number (L_F) for $U_0 = 0$

Since the maximum variation in temperature departures is observed in stagnant air, the temperature departures for different Lewis numbers at $U_0 = 0$ is presented in Fig. 3. As expected $Z_s - \xi_f > 0$ for Lewis numbers lesser than one and $Z_s - \xi_f < 0$ for Lewis numbers greater than one. For $L_f \to 0$ (at $Z_s = 0.75$) , $Z_s - \xi_f \approx 0.8$ which indicates that flame temperatures 80% greater than the adiabatic flame temperatures are encountered. As L_F increases from 0 to 1 the $|Z_s - \xi_f|$ decreases and on increasing beyond 1, the $|Z_s - \xi_f|$ starts to increase again. For $L_f = 3.0$ at $Z_s = 0.14$, $Z_s - \xi_f \approx -0.2$ indicating flame temperature is subadiabatic by 20%. For $L_F \to 0$ the maximum temperature departures occur at $Z_s = 0.75$ whereas for $L_F = 3$ the maximum temperature departures occur at $Z_s = 0.1$. This indicates that, with increase in Lewis number the value of Z_s at which the temperature departure is maximum decreases. This implies that the differential diffusion effects are more pronounced at higher dilution for lower Lewis numbers, whereas for higher Lewis numbers they are more dominant at lower dilutions.

2.5 Modified Equations for Computation

The solution obtained for small x (x<<1) is used as initial condition for the solving the conservation equations. However the location of flame is not known, to make the numerical computation simpler, a re-scaled coordinate is introduced, $R = r/r_f(x)$ where $r_f(x)$ is the flame location that changes with x. The coordinates are changed from (x, r) $\rightarrow (x, R)$ and in the new coordinates the flame location is always at $R = 1$. The continuity and momentum equations in the new coordinates are

$$\frac{\partial U}{\partial x} - \frac{R}{r_f}\frac{\partial r_f}{\partial x}\frac{\partial U}{\partial R} + \frac{1}{r_f}\frac{1}{R^j}\frac{\partial}{\partial R}(R^j V) = 0 \tag{2.49}$$

$$U\frac{\partial U}{\partial x} - U\frac{R}{r_f}\frac{\partial r_f}{\partial x}\frac{\partial U}{\partial R} + \frac{V}{r_f}\frac{\partial U}{\partial R} = \frac{Pr}{r_f^2}\frac{1}{R^j}\frac{\partial}{\partial R}(R^j\frac{\partial U}{\partial R}) \tag{2.50}$$

The boundary conditions are

$$\begin{cases} R = 0: \quad V = \frac{\partial U}{\partial R} = 0 \\ R = \infty : U = U_0 \end{cases} \tag{2.51}$$

The mixture fraction equation can be separated into two domains $[0, 1]$ and $[1, \infty]$ with $\tilde{Z} = \tilde{Z}_s$ as the boundary condition at the interface of the two domains. Using the relation between Z and $\tilde{Z}$ from the equation (2.14) the equation for the domain [0 1] is

$$U\frac{\partial \tilde{Z}}{\partial x} - U\frac{R}{r_f}\frac{\partial r_f}{\partial x}\frac{\partial \tilde{Z}}{\partial R} + \frac{V}{r_f}\frac{\partial \tilde{Z}}{\partial R} = \frac{1}{L_{\mathrm{F}} r_f^2}\frac{1}{R^j}\frac{\partial}{\partial R}(R^j\frac{\partial \tilde{Z}}{\partial R}) \tag{2.52}$$

and the boundary conditions are

$$\begin{cases} R = 0: \quad \frac{\partial \tilde{Z}}{\partial R} = 0 \\ R = 1: \quad \tilde{Z} = \tilde{Z}_s \end{cases} \tag{2.53}$$

The equation for the domain $[1, \infty]$ is

$$U\frac{\partial \tilde{Z}}{\partial x} - U\frac{R}{r_f}\frac{\partial r_f}{\partial x}\frac{\partial \tilde{Z}}{\partial R} + \frac{V}{r_f}\frac{\partial \tilde{Z}}{\partial R} = \frac{1}{r_f^2}\frac{1}{R^j}\frac{\partial}{\partial R}(R^j\frac{\partial \tilde{Z}}{\partial R}) \tag{2.54}$$

the boundary conditions are $\tilde{Z} = \tilde{Z}_s$ at $R = 1$ and $\tilde{Z} = 0$ at $R \rightarrow \infty$. The equations (2.49) (2.50) (2.51) (2.52) along with their boundary conditions are solved numerically,

the following condition is applied to find r_f.

$$\frac{\partial \tilde{Z}}{\partial R}\Big|_{1-} = \frac{\partial \tilde{Z}}{\partial R}\Big|_{1+} \tag{2.55}$$

Once r_f is found the temperature at the flame can be computed by solving the following enthalpy equation and evaluating ξ at R=1

$$U\frac{\partial \xi}{\partial x} - U\frac{R}{r_f}\frac{\partial r_f}{\partial x}\frac{\partial \xi}{\partial R} + \frac{V}{r_f}\frac{\partial \xi}{\partial R} = \frac{1}{r_f^2}\frac{1}{R^j}\frac{\partial}{\partial R}(R^j\frac{\partial \xi}{\partial R}) \tag{2.56}$$

and the boundary conditions are

$$\begin{cases} R = 0: & \frac{\partial \xi}{\partial R} = 0 \\ R = \infty: & \xi = 0 \end{cases} \tag{2.57}$$

Chapter 3

Results and Discussion

The results obtained from modeling are presented in this section. The effect of three parameters namely the Lewis number (L_{F}), fuel dilution (S) and the coflow velocity (U_0) are discussed. Mainly two Lewis numbers $L_{\text{F}} = 0.3$ and $L_{\text{F}} = 2$ are considered. $L_{\text{F}} = 0.3$ represents the properties of hydrogen and $L_{\text{F}} = 2.0$ corresponds to that of heavy hydrocarbons. Five different fuel dilutions are examined for each Lewis number. Four different coflow-to-jet velocity ratios $U_0 = 0$ (stagnant air), 0.5, 1 and 2 are selected. The effect of these parameters on flame shapes and temperature departures ($Z_s - \xi_f$) are analyzed. The shape of the flame is characterized mainly by the flame length and flame width. Flame length is defined as the axial distance from the exit of the injector to the location where $Z = Z_s$ (or $\tilde{Z} = \tilde{Z}_s$) on the axis. Flame width is defined as the maximum radial distance between the axis of symmetry and the flame location. All the results presented in this section are for an axisymmetric configuration, the planar configuration results are presented in Appendix.

3.1 Effect of Lewis Number

To investigate the effect of Lewis number, the flame shapes and flame temperatures of five Lewis numbers $L_{\text{F}} = 0.3$, 0.75, 1.0, 2.0 and 3.0 are computed and presented in Fig. 4. The flame shapes shown in the upper plot of Fig 4 reveal that for smaller L_{F} the flame is radially outward and as L_{F} increases the flame width decreases and the flame

length increases. Lewis number is the ratio of thermal diffusivity to mass diffusivity and as Lewis number increases the mass diffusivity decreases. When mass diffusivity is larger, the flame diffuses to larger distances which results in larger flame width. For larger L_{F} the mass diffusivity is reduced, so the diffusion is slower and the fuel diffuses to smaller radial distances resulting in smaller flame widths. As the diffusion is slower the flame would require larger axial distance to diffuse that results in larger flame lengths.

The temperature departures along the flame for various Lewis numbers are shown in the lower plot of Fig. 4. The initial flame temperatures for L_{F} less than one/equal to one/greater than one are superadiabatic/adiabaitc/ subadiabaitc respectively. For $L_{\mathrm{F}} = 1.0$, the rate of heat transfer is equal to the rate of mass transfer and as a result the flame temperature is adiabatic, whereas for $L_{\mathrm{F}} = 0.3$ the smaller rate of heat transfer leads to a superadiabatic flame temperature and inversely for $L_{\mathrm{F}} > 1.0$ the larger rate of heat loss gives rise to a subadiabatic flame temperature. For Lewis numbers smaller than one the flame temperatures downstream become subadiabatic, whereas for Lewis number greater than one the flame temperatures undergo transition from subadiabatic to superadiabatic. As expected for Lewis number equal to one $Z_s - \xi_f = 0$ along the entire flame, indicating that the flame temperature is always adiabatic i.e $T_f = T_S$. This is because for $L_{\mathrm{F}} = 1$, $\xi_f = Z_s = 1/(S+1)$. However for $L_{\mathrm{F}} > 1$, ξ_f is initially greater than Z_s and decreases along the flame and eventually decreases to a value lower than Z_s. In the case of $L_{\mathrm{F}} < 1$, ξ_f increases along the flame that results in the transition from super to subadiabatic flame temperatures. The point where the transition occurs is the point where the flame of a given Lewis number intersects the flame shape of $L_{\mathrm{F}} = 1$.

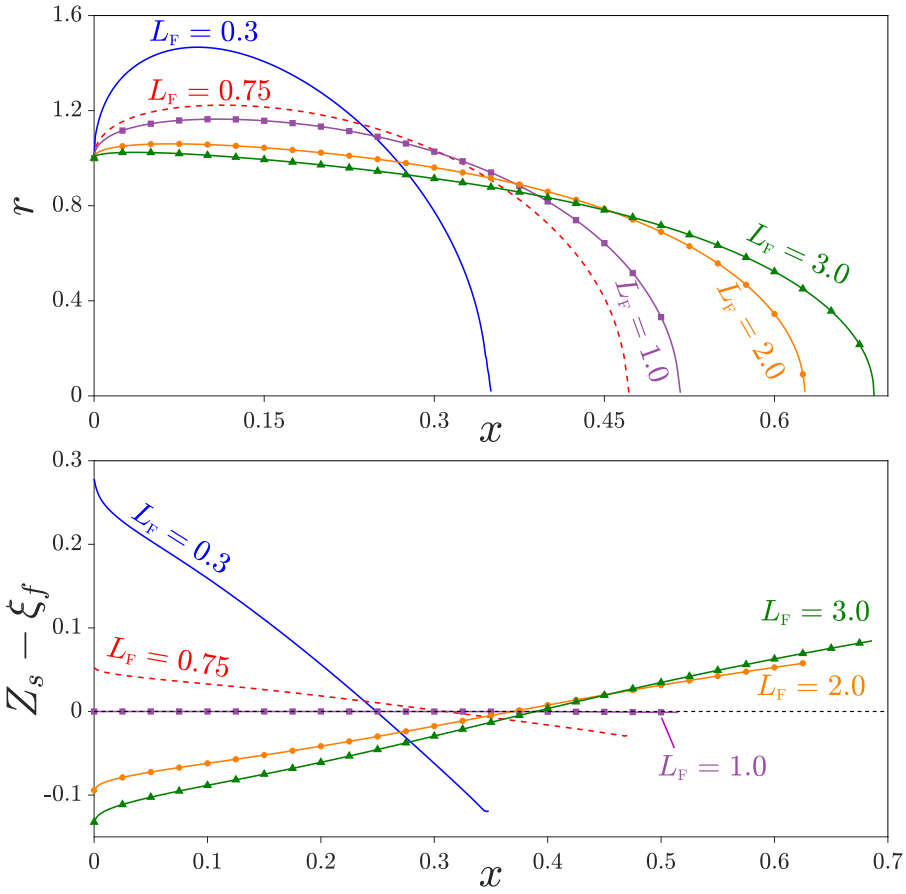

Figure 4: The flame shapes (upper plot) and dimensionless excess temperatures $Z_s - \xi_f$ (lower plot) for different Lewis numbers with $S = 1.0$ in stagnant air i.e $U_0 = 0$.

3.2 Effect of Dilution

Diluting the fuel with inert gasses such as nitrogen significantly effects the soot formation as reported by many researchers [37, 40, 59], hence it is necessary to understand the effects of fuel dilution on flame structure and flame temperature. For a Lewis number (L_F) of 0.3, the different values of S considered are $S = 0.5$, 1.0, 2.0, 8.0 and 34.5, where $S = 0.5, 1.0, 2.0$ represent extremely diluted fuels and $S = 8$, 34.5 correspond to undiluted hydrogen-air mixture and undiluted hydrogen respectively.

The flame shapes in stagnant air $U_0 = 0$ for $L_F = 0.3$ and $L_F = 2.0$, are shown in left and right plots of Fig. 5 respectively. It is observed that as the dilution increases

(or S decreases) the flame length decreases. As S decreases the $\tilde{Z}_s$ increases and this higher value of $\tilde{Z}_s$ would be achieved earlier. Linan et al. [17] have reported that for highly diluted fuels (S of the order 1) the flame length is of order L_d and $\tilde{Z}$ decreases axially as L_d/x, where L_d ($L_d = Re\ a$) is the jet development length. However for undiluted fuels (large S) the flame length is of the order SL_d. Diluted fuels exhibited lower flame height and width whereas much larger values were observed for undiluted fuels. This is because diluted fuels have smaller amount of fuel which would undergo combustion in shorter duration leading to smaller flame lengths and flame width whereas for larger S (lower Z_s) the combustion occurs over a larger area and resulting in a larger flame. For undiluted fuels the diffusion is slower and a larger length is require for the $\tilde{Z}$ to decay to the value $\tilde{Z}_s$. Roper [8] and Sunderland [14] have attributed the reduced mass diffusivities for larger flame lengths. As a consequence greater radial convection is observed for undiluted fuels which in-turn explains the radially outward nature of flame. For $L_{\text{F}} = 2.0$, the five dilutions considered are $S = 0.5$, 1, 2, 3.43 and 15. $S = 0.5, 1.0, 2.0$ represent extremely diluted fuels and $S = 3.43$ and 15 represent the heavy hydrocarbon-air mixture and undiluted heavy hydrocarbons respectively. A similar trend is observed in flame shapes for $L_{\text{F}} = 2.0$, as the dilution increases the flame length and flame width decrease attributed to the lower fraction of fuel that has to undergo combustion. The flame shapes obtained for $L_{\text{F}} = 2.0$ are elongated and exhibit larger flame lengths than the corresponding $L_{\text{F}} = 0.3$ due to their smaller mass diffusivities.

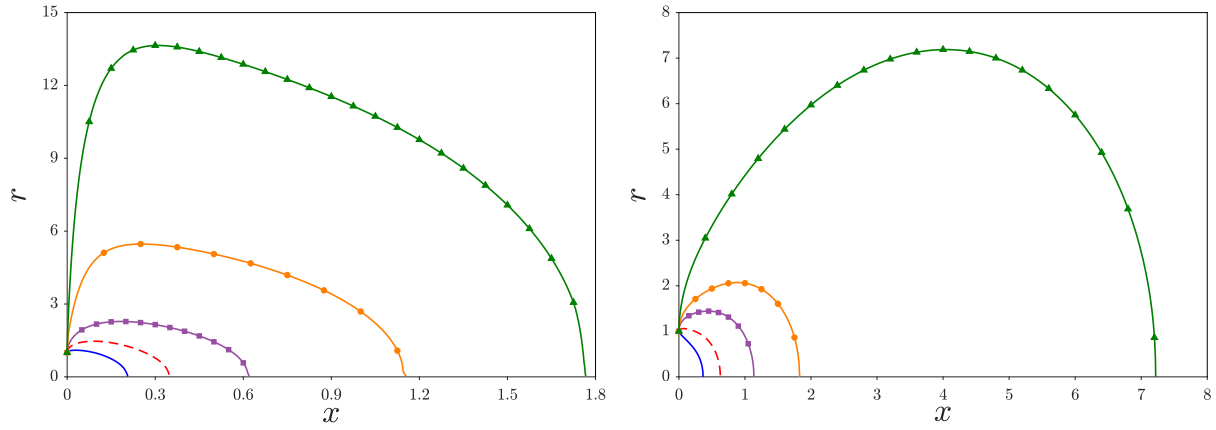

Figure 5: The flame shapes of $L_{\mathrm{F}} = 0.3$ (left) and $L_{\mathrm{F}} = 2.0$ (right) for different fuel dilutions in stagnant air i.e $U_0 = 0.0$

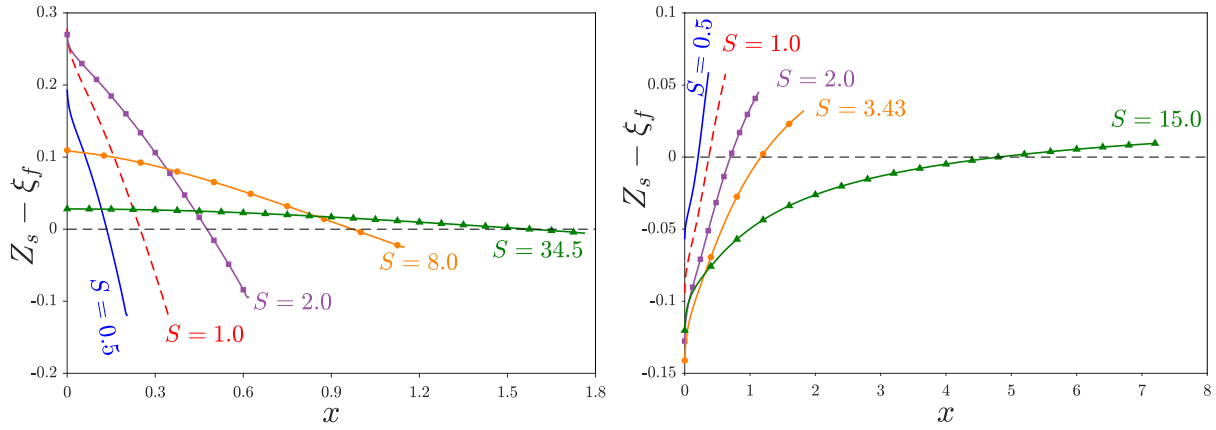

Figure 6: The dimensionless excess temperatures $Z_s - \xi_f$ of $L_{\mathrm{F}} = 0.3$ (left) and $L_{\mathrm{F}} = 2.0$ (right) for different fuel dilutions in stagnant air i.e $U_0 = 0$

The temperature departures $Z_s - \xi_f$ along the flame for $L_{\mathrm{F}} = 0.3$ and $L_{\mathrm{F}} = 2.0$ are shown in the left and right plot of Fig. 6. The flame temperature for $L_{\mathrm{F}} = 0.3$ is maximum at the exit of the injector and decreases from there onwards. For all the different dilutions the initial value $Z_s - \xi_f$ is positive which indicates a superadiabatic flame temperature. The differential diffusion of hydrogen results in the faster diffusion of H_2 towards the oxidizer side and this results in an increased mass fraction of hydrogen at lower values of Z (outside the flame) and a decreased mass fraction of hydrogen at higher values of Z (inside the flame) [32] which causes the flame to shift towards the side of the oxidizer resulting in superadiabatic flame temperatures. The flame temperature decreases in direction of flow

this is because the excess enthalpy variable at the flame (ξ_f) increases and consequently $Z_s - \xi_f$ decreases. The temperature departures keep decreasing and at a certain location the flame temperature undergoes transition from superadiabatic to subadiabatic. The transition from superadiabatic to subadiabatic flame temperatures is observed irrespective of the values of S, however as S increases the transition is delayed. This implies that a larger potion of the flame is subadiabatic for smaller S and a smaller portion of the flame is subadiabatic for larger S. For S = 8 and 34.5, subadiabatic temperatures are observed only near the tip of the flame. The initial values of the temperature departures $Z_s - \xi_f$ observed for $L_{\text{F}} = 2.0$ are smaller than zero which increases in the direction of flow. The differential diffusion of hydrocarbons has an inverse effect to that of the hydrogen which results in subadiabatic temperature at the injector rim [32]. As we move along the flame, the temperature increases and subsequently a superadiabatic temperature is achieved. The transition from subdiabatic to superadiabatic flame temperatures is observed for all S and for heavy hydrocarbon-air mixtures ($S = 15$) the flame is superadiabatic only near the tip. The flame shapes for $L_{\text{F}} = 0.3$, and $L_{\text{F}} = 2.0$ in the excess enthalpy variable field are shown in Fig 7. The colored region represents $\xi > Z_s$ whereas outside it $\xi < Z_s$, so when the flame lies in the colored region then it is subadiabatic and when it lies outside the colored region it is superadiabaic. The equation (2.30) is independent of Lewis number of fuel so when the flame is outward as in the case $L_{\text{F}} = 0.3$, ξ is lower than Z_s. This results in positive values for the temperature departures, which correspond to superadiabatic flame temperatures. Moving downstream the transition from super to subadiabatic takes place at the location where the flame shape crosses the curve $\xi = Z_s$ (the flame shape of $L_{\text{F}} = 1.0$). Subsequently the enthalpy variable is greater than the Z_s that gives rise to subadiabatic flame temperatures. The flame shape for $L_{\text{F}} = 2.0$ is radially inward and inside the curve $\xi = Z_s$ so the excess enthalpy variably is greater than Z_s which causes subadiabatic temperatures. However as we move downstream the flame shape of $L_{\text{F}} = 2.0$ crosses the curve $\xi = Z_s$, at this location the sign of the temperature departures is reversed and now $Z_s - \xi_f > 0$, resulting in superadiabaitc temperatures.

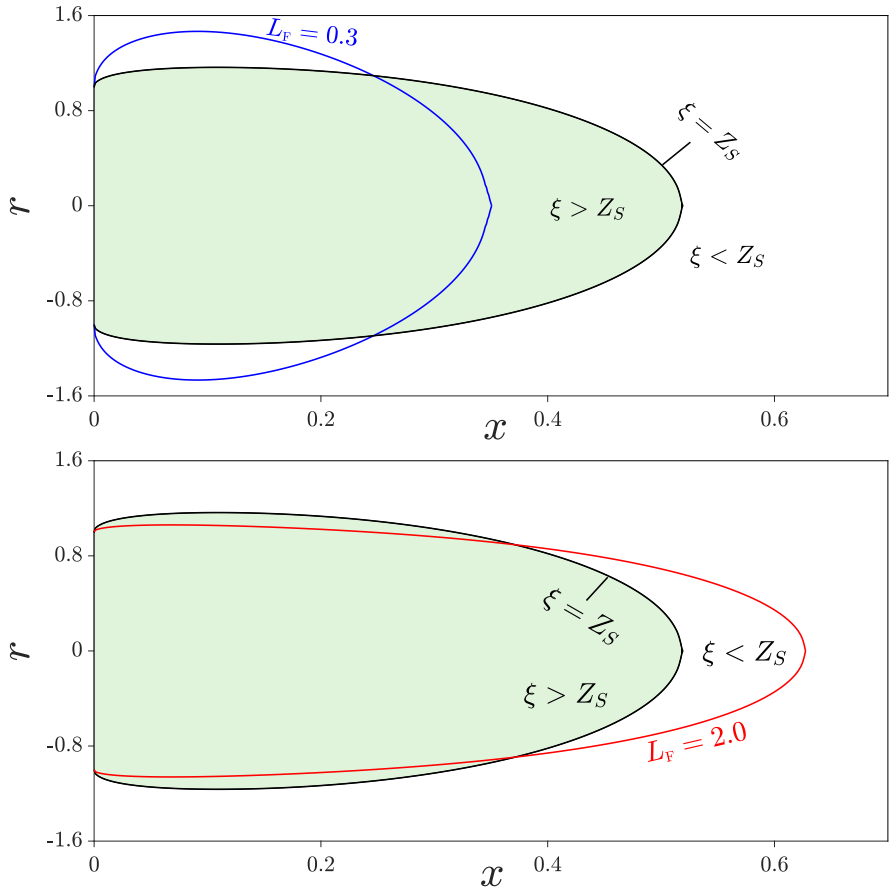

Figure 7: The flame shape of $L_F = 0.3$ (upper plot) and $L_F = 2.0$ (lower plot) in the excess enthalpy variable field with $S = 1$ and $U_0 = 0$. In the colored region $\xi > Z_s$

The unexpected behaviour of transition between superadiabatic /subadiabatic is further emphasized by the profiles of Z, ξ for $S = 1$ in Fig. 8. For $L_F = 0.3$ the value of ξ_f increases as we move along the flame and at $x = 0.25$, $Z_s = \xi_f$, this is the location at the which the flame temperature undergoes transition from super to subadiabatic. However the value of the excess enthalpy variable at the flame for $L_F = 2.0$ decreases and consequently $Z_s - \xi_f$ increases. For $L_F = 2.0$, the transition from sub to superadiabatic occurs at $x = 0.37$.

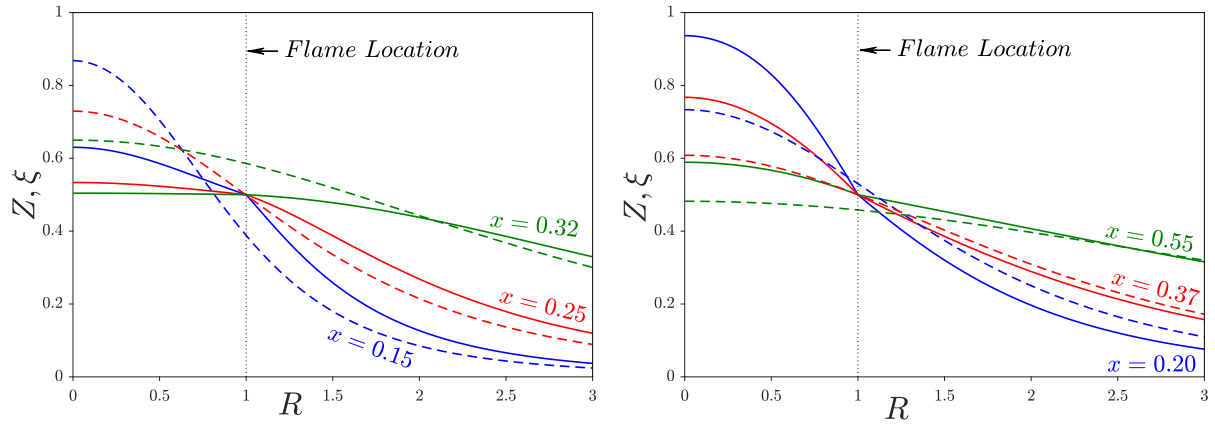

Figure 8: The Z, ξ profiles at different axial locations with $S = 1$ and $U_0 = 0$ for $L_{\text{F}} = 0.3$ (left) and $L_{\text{F}} = 2.0$ (right)

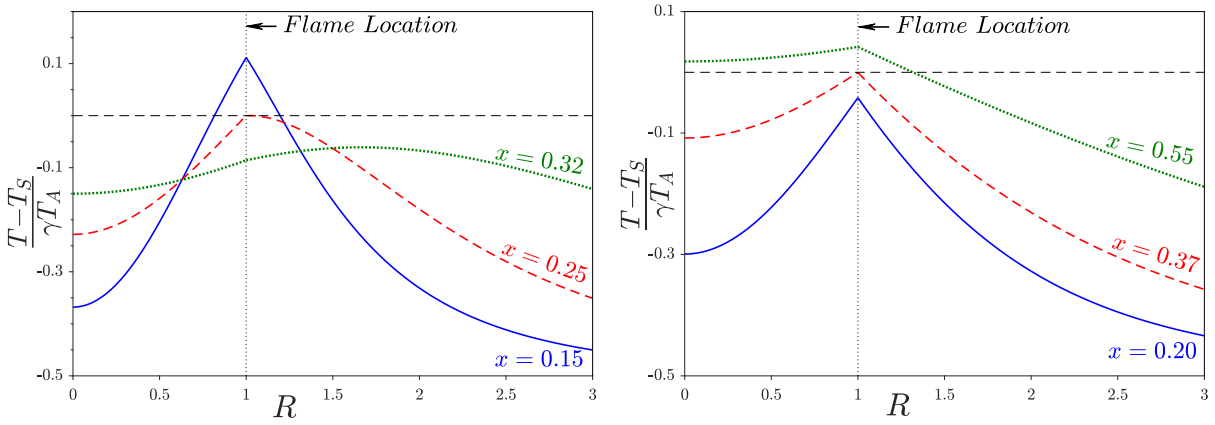

Figure 9: The temperatures profiles at different axial locations with $S = 1$ and $U_0 = 0$ for $L_{\text{F}} = 0.3$ (left) and $L_{\text{F}} = 2.0$ (right)

The temperature profiles at different axial locations are shown in Fig. 9. For $L_{\text{F}} = 0.3$, the flame moves towards the fuel side rapidly, where the oxygen available for combustion is reduced, which results in the decrease of the flame temperature. The flame temperature keeps decreasing in the axial direction and eventually there comes a point ($x = 0.32$) where the maximum temperature is no longer at the flame but is on the oxidizer side. This observation is a consequence of the differential-diffusion effects of H_2 However there is no such observation for $L_{\text{F}} = 2.0$. The maximum temperature is always at the flame for all axial locations. As explained by researchers [18] the peak temperature is at the flame because the heat loss is positive on both sides of the flame. This implies that differential-

diffusion effects are not large enough to displace the peak temperatures to the fuel side for heavy hydrocarbons. Larger differential-diffusion effects are present for $L_{\text{F}} = 0.3$ that cause the peak temperature to be displaced towards side the oxidizer. This indicates that the differential diffusion effects for $L_{\text{F}} = 0.3$ are greater than $L_{\text{F}} = 2.0$ for $S = 1$.

3.3 Effect of Coflow Velocity

In this section the effect of coflow velocities on flame shapes and temperature departures are analyzed. An advantage of a larger coflow air velocity is its ability to reduce the Nitrous oxide (NO_x) levels [41, 42, 43] so it is important to understand the effects of coflow velocity. Four different coflow to jet velocity ratios $U_0 = 0.0, 0.5, 1.0, 2.0$ are considered. The Fig 10 shows the flame shapes for $L_{\text{F}} = 0.3$ (left plot) and $L_{\text{F}} = 2.0$ (right plot) with $S = 1$. The flame is the largest in stagnant air conditions ($U_0 = 0$) and as the velocity of air increases the flame length and the flame width decreases. For larger coflow to jet velocity ratios (U_0), the velocity of the coflowing air causes a confinement effect, which increase as the velocity of air increases. Greater confinement effect, results in a smaller flame width and flame length. In case of smaller U_0 the diffusion is slower and the fuel would advect to larger distances downstream which results in larger flame lengths. Dahm [44] and Chen et al. [28] reported that larger coflow velocity would reduce the amount of entertainment air required to dilute the fuel to stoichiometric proportions. As U_0 increases the radial convection decreases that contributes in the reduction of the flame width. The flame shapes exhibit similar trends for $L_{\text{F}} = 0.3$ and $L_{\text{F}} = 2.0$. The only difference being $L_{\text{F}} = 2.0$ show slightly elongated flame shapes i.e larger flame length and smaller flame width which is a result of their smaller mass diffusivities.

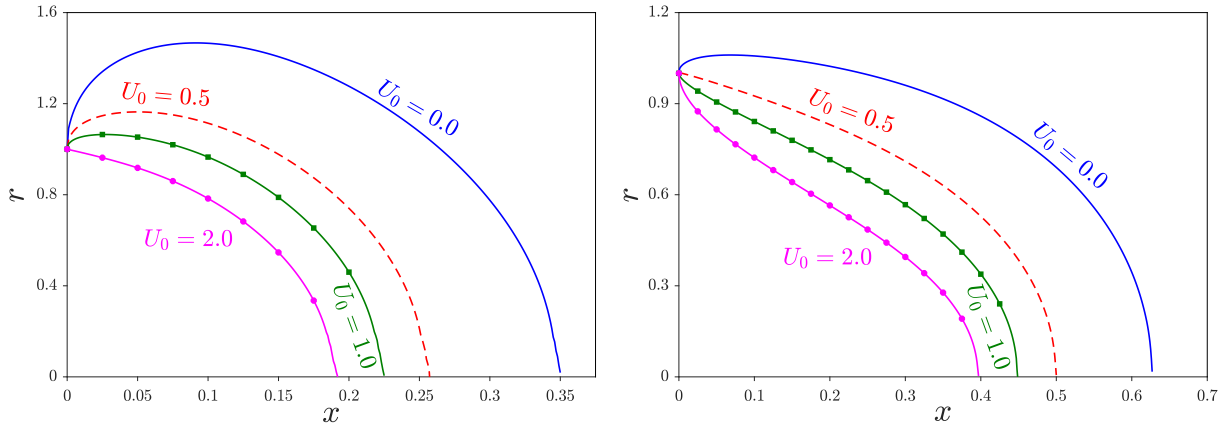

Figure 10: The flame shapes of $L_{\rm F} = 0.3$ (left) and $L_{\rm F} = 2.0$ (right) for different coflow velocities with with $S = 1$

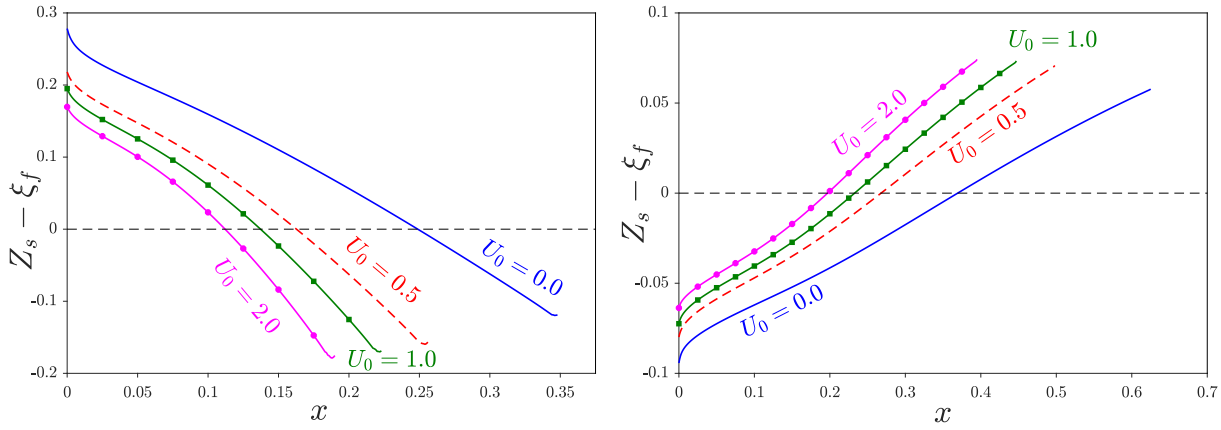

Figure 11: The dimensionless excess temperatures $Z_s - \xi_f$ of $L_{\rm F} = 0.3$ (left) and $L_{\rm F} = 2.0$ (right) for different coflow velocities with S=1

The temperature departures in Fig 11 indicate that on increasing the coflow velocity the transition from super to subadiabatic flame temperature for $L_{\rm F} = 0.3$ and sub to superadiabatic flame temperatures for $L_{\rm F} = 2.0$ takes place earlier. Flows with higher U_0 exhibit a larger fraction of the flame that has a subadiabatic/superadiabatic flame temperature for $L_{\rm F} = 0.3$ and $L_{\rm F} = 2.0$ respectively. Differential diffusion effects are greater for smaller U_0 that result in a larger value of $|Z_s - \xi_f|$ near the rim of the injector ($x = 0$). With increase in coflow velocity the flame moves more rapidly towards the fuel side which causes the flame temperature to undergo transition at an earlier downstream location. It is also observed that for smaller U_0 the difference in flame temperature at

the injector exit and the flame tip is greater, a possible reason for this is the larger flame length.

3.4 Inverse Diffusion Flames

Inverse diffusion flames are similar to normal diffusion with the only difference that the air stream and fuel stream are interchanged, now air flows through the central tube and fuel flows in the annulus. The governing equation for the inverse diffusion flames are (2.28), (2.29) , (2.30) and (2.31) that must be integrated along with the following initial and boundary conditions

$$x = 0 \begin{cases} Z = \tilde{Z} = \xi = U - U_0 = 0 & \text{for } r \leq 1 \\ Z = \tilde{Z} = \xi = 1,\ U = 1 & \text{for } r \geq 1 \end{cases} \tag{3.1}$$

$$x > 0 \begin{cases} r = 0: \quad V = \frac{\partial U}{\partial r} = \frac{\partial Z}{\partial r} = \frac{\partial \tilde{Z}}{\partial r} = \frac{\partial \xi}{\partial r} = 0 \\ r = \infty: \quad Z = \tilde{Z} = \xi = 1, \quad U = 1 \end{cases} \tag{3.2}$$

The relations in (2.14) and (2.15) can be used in combination to solve the above equations. The resulting flame shapes and temperatures departures for $L_{\text{F}} = 0.3$ and $L_{\text{F}} = 2.0$ are presented in Fig. 12 and Fig 13 respectively for coflow-to-jet velocity ratio of unity i.e $U_0 = 1$. Fig. 12 shows that as dilution increases the flame length and flame width increases. In inverse diffusion flames the oxidizer is deficient and fuel is abundant. When the dilution is low there is sufficient amount of fuel and oxidizer which would undergo combustion faster. Increase in dilution would decrease the amount of fuel, and as the deficient reactant is the oxidizer the combustion between smaller quantities of fuel and oxidise would take longer time and over a larger area. Accordingly the flame length and width would be larger for higher dilution. Also for lower dilution, the mixing of fuel and oxidizer is faster and the fuel is burned faster leading to smaller flame lengths whereas for larger dilution the mixing of flame and air is slower and the combustion would take more time leading to larger flames. Mathematically this can be seen as follows, Z has to increase to the value of Z_s on the axial location and for larger dilution Z_s is larger, hence Z achieves Z_s at a later axial location. Sze et al [60] have explained the degree of entrainment as a major factor in determining the flame length and as the entrainment

increases the mixing and the fuel would be burned in a premixed mode and this would result in a faster combustion and smaller flame lengths.

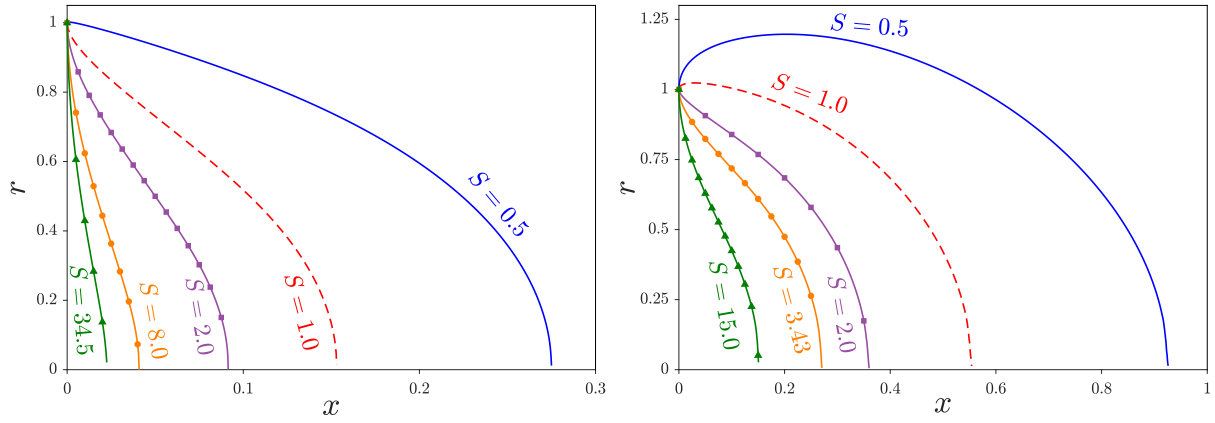

Figure 12: The flame shapes of inverse diffusion flame of $L_{\mathrm{F}} = 0.3$ (left) and $L_{\mathrm{F}} = 2.0$ (right) for different fuel dilutions with coflow to jet velocity ratio of $U_0 = 1.0$

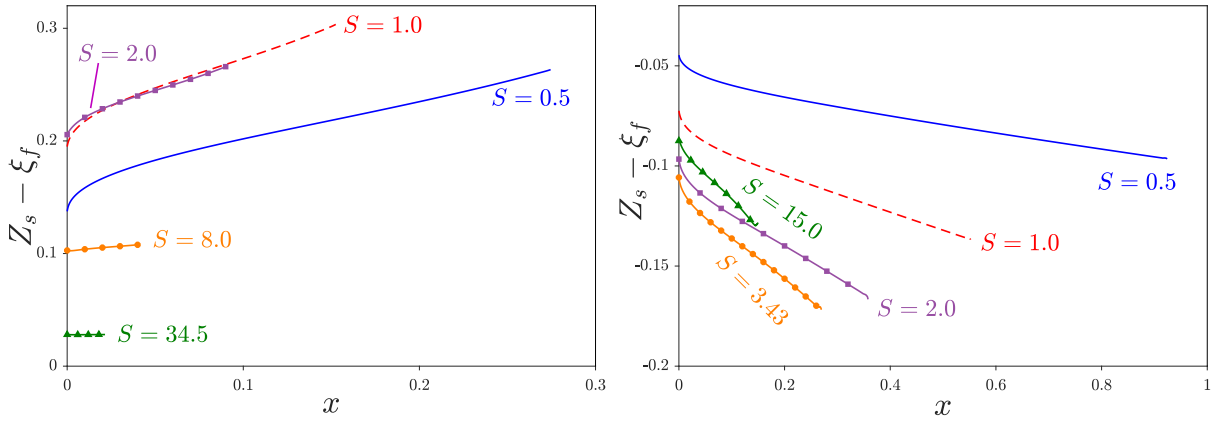

Figure 13: The dimensionless excess temperatures $Z_s - \xi_f$ of inverse diffusion flame of $L_{\mathrm{F}} = 0.3$ and $L_{\mathrm{F}} = 2.0$ for different fuel dilutions with coflow to jet velocity ratio of $U_0 = 1.0$

The temperature departures of $L_{\mathrm{F}} = 0.3$ and $L_{\mathrm{F}} = 2.0$ are shown in left and right plots of Fig. 13 respectively. The temperature departures indicate that the flame temperatures are always superadiabatic for $L_{\mathrm{F}} = 0.3$. The flame temperatures increase downstream and reach a maximum at the tip of the flame. Whereas for $L_{\mathrm{F}} = 2.0$ the flame temperatures are always subadiabatic and decrease along the flame and are minimum at the flame tip. This is in contrast to the nontrivial behaviour observed in normal diffusion flames. This

suggests that the diffusivity of the deficient reactant in the central-jet is more important than the diffusivity of the abundant (coflow) reactant.

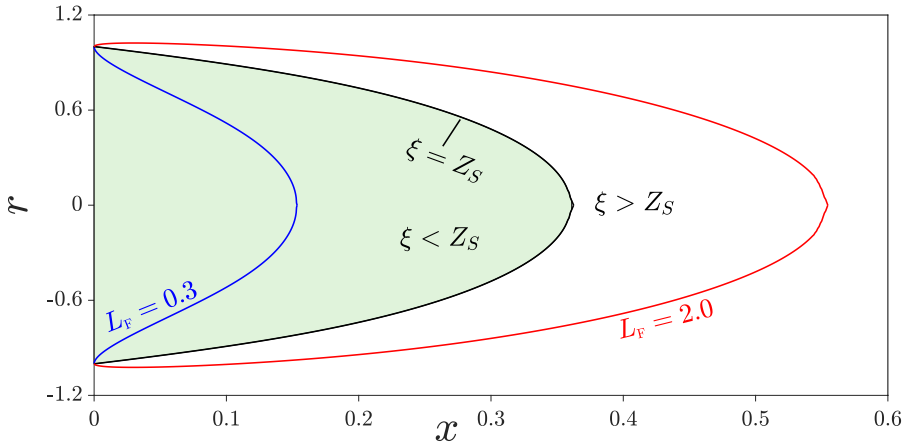

Figure 14: The flame shapes of inverse diffusion flames in the enthalpy variable field for $L_F = 0.3$ and 2.0 with $S = 1$ and $U_0 = 1$.

The flame shapes for $L_F = 0.3$, and 2.0 are shown in Fig. 14. The curve $\xi = Z_s$ corresponds to the flame shape of $L_F = 1.0$. The excess enthalpy variable inside the flame of $L_F = 1.0$ ($\xi = Z_s$) is smaller than Z_s (i.e $\xi < Z_s$) and is larger in the region outside $\xi > Z_s$. The entire flame of Lewis number two lies in the region $\xi > Z_s$ and Lewis number 0.3 in the region $\xi < Z_s$. This implies that for $L_F = 0.3$,the temperatures departures is always greater than zero and for $L_F = 2.0$ the temperatures departures are always less than zero. This results in superadiabatic temperatures for $L_F = 0.3$ and subadiabatic temperatures for $L_F = 2.0$. This is further confirmed by the profiles of Z, ξ for $L_F = 0.3$ and 2.0 in Fig 15. ξ profiles for $L_F = 0.3$ reveal that ξ_f decreases along the axial direction and consequently $Z_s - \xi_f$ increases, which leads to higher flame temperatures near the tip. In contrast, the ξ_f increases for $L_F = 2.0$ resulting in a decrease of flame temperatures downstream. The temperature profiles at three different axial locations for $S = 1$ are shown in Fig. 16. They show that the maximum temperature is always at the flame location. The flame temperature increases along the axial direction for $L_F = 0.3$ and as a result the maximum flame temperatures is observed at the flame ti. Whereas the flame temperatures decreases downstream in case of $L_F = 2.0$ and consequently the flame

temperature is lowest at the flame tip.

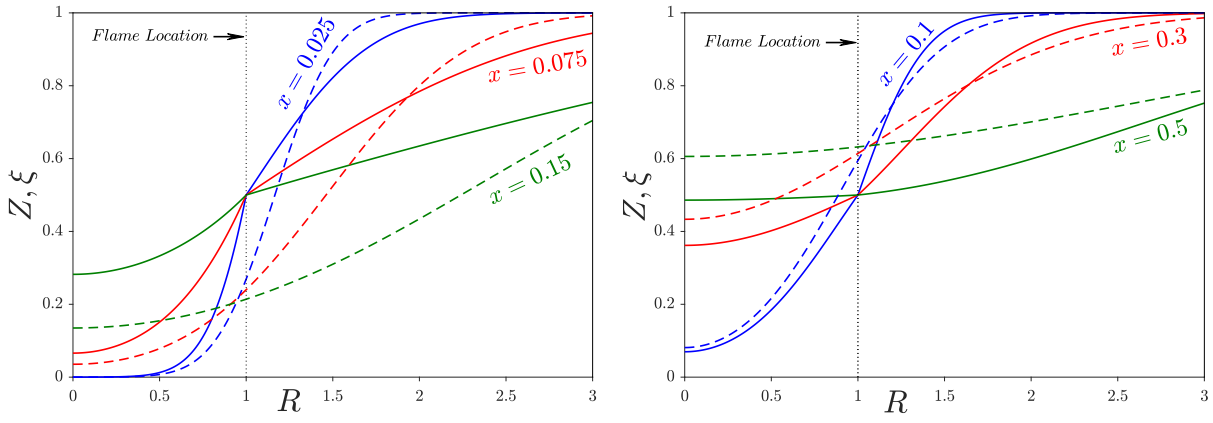

Figure 15: The Z, ξ profiles of inverse diffusion flames at different axial locations with $S = 1$ and $U_0 = 1.0$ for $L_{\text{F}} = 0.3$ and $L_{\text{F}} = 2.0$ (right)

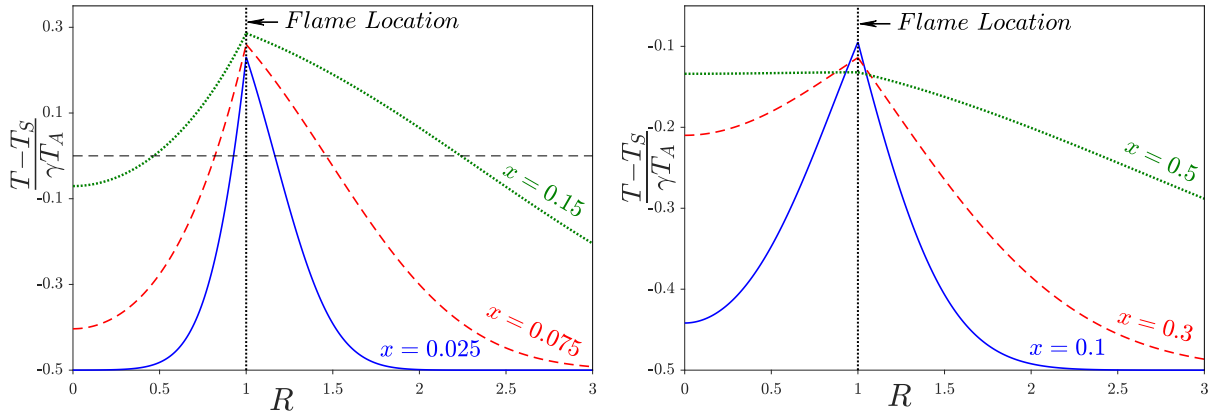

Figure 16: The temperatures profiles of inverse diffusion flames at different axial locations with $S = 1$ and $U_0 = 1.0$ for $L_{\text{F}} = 0.3$ (left) and $L_{\text{F}} = 2.0$ (right)

Chapter 4

Conclusion

Numerical computations of laminar jet diffusion flames were carried out by applying the Burke-Schumann limit for different dilutions (S), Lewis number (L_{F}) and coflow-to-jet velocity ratios (U_0). Differential-diffusion effects are found to be more pronounced in stagnant air ($U_0 = 0$) and diminish as U_0 increases. These effects are found to be maximum at intermediate values of stoichiometric mixture fraction $Z_s = 1/(S + 1)$ corresponding to S values of order unity. It is inferred from Fig. 2 that for $S \approx 1.5$, superadiabatic temperature increment of 25% is observed for $L_{\text{F}} = 0.3$, whereas for $S \approx 4$, subadiabatic temperature decrements of 14% are experienced for $L_{\text{F}} = 2.0$. As $L_{\text{F}} \to 0$ superadiabatic temperatures of about 80% are observed at $S \approx 0.33$ and for $L_{\text{F}} = 3.0$, subadiabatic temperatures of 20% is encountered at $S \approx 6$. From these observations it can be concluded that as the Lewis number increases the differential-diffusion effects are more pronounced at lower dilutions (i.e larger values of S).

Larger Lewis number resulted in larger flame length and smaller flame width attributed to their reduced mass diffusivities. Fuel dilution decreased the flame length and flame widths. Dilution decreased the fraction of fuel that resulted in smaller flames. For $L_{\text{F}} < 1$ on moving downstream the superadiabatic flames temperatures underwent transition to subadiabatic, whereas for $L_{\text{F}} > 1$ in the flow direction the flames temperatures evolved from subadiabatic to superadiabatic flame temperatures. This change in nature of the jet-flame temperature has been reported for the first time. While in other configurations such as flame vortices, this non-trivial behaviour was restricted to small values of S ($S < 1$),

for jet flames the subadiabatic/superadiabtic transition occurs irrespective of the value of S. Under these conditions the peak temperatures are displaced and no longer occur at the flame sheet. Results in Figs 10 and 11 show that as coflow velocity increases the confinement effect causes a decrease in the flame length and flame width. The transition in flame temperatures takes place earlier and a larger fraction of the flame length exhibits the superadiabatic/subadiabatic nature.

Inverse diffusion flames were modeled for $L_{\text{F}} \neq 1$ and different fuel feed dilutions. The results showed that as the fuel dilution increased the flame length and flame width increased. For $L_{\text{F}} < 1$ the flame temperatures are maximum at the tip of the flame, whereas for $L_{\text{F}} > 1$ they are minimum at the flame tip. The flame temperature increased along the axial direction and remained superadiabatic/subadiabatic over the entire flame length for $L_{\text{F}} = 0.3/2.0$. The unexpected behavior of the flame temperature is not present in inverse diffusion flames.

Appendix A

Additional Results

In this section additional results are presented. These include the results of different dilutions for a unity coflow to jet velocity ratio $U_0 = 1$ for axisymmetric configuration. In addition to this, the results for a planar case are also presented. The planar case results comprises of the effect of Lewis number, dilution, coflow velocity and inverse diffusion flames. Similar trends are observed for the planar configuration as the axisymmetric configuration and hence very little explanation is given here. For a better and detailed explanation refer to the results and discussion (chapter 3).

A.1 Axisymmetric Results

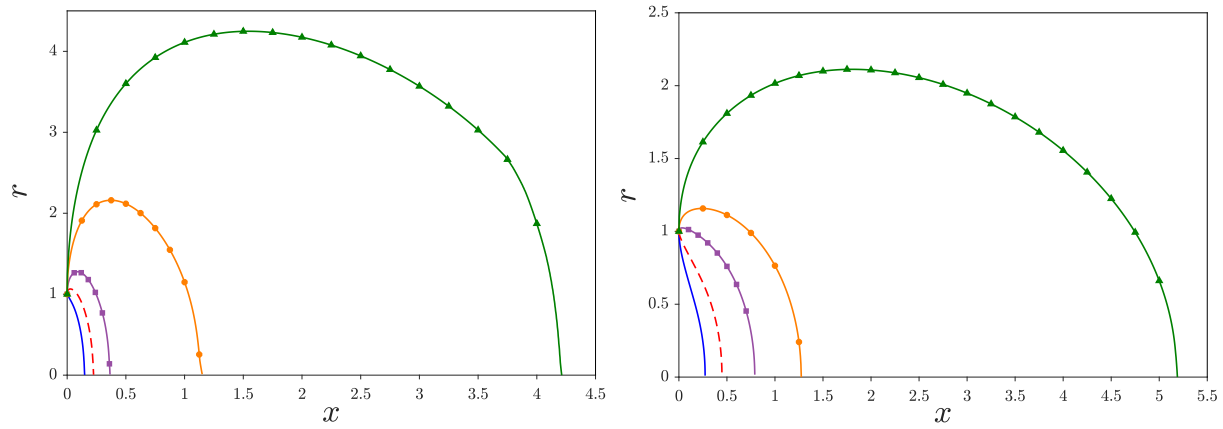

Figure 17: The flame shapes for $L_{\mathrm{F}} = 0.3$ (left) and $L_{\mathrm{F}} = 2.0$ (right) with $U_0 = 1.0$

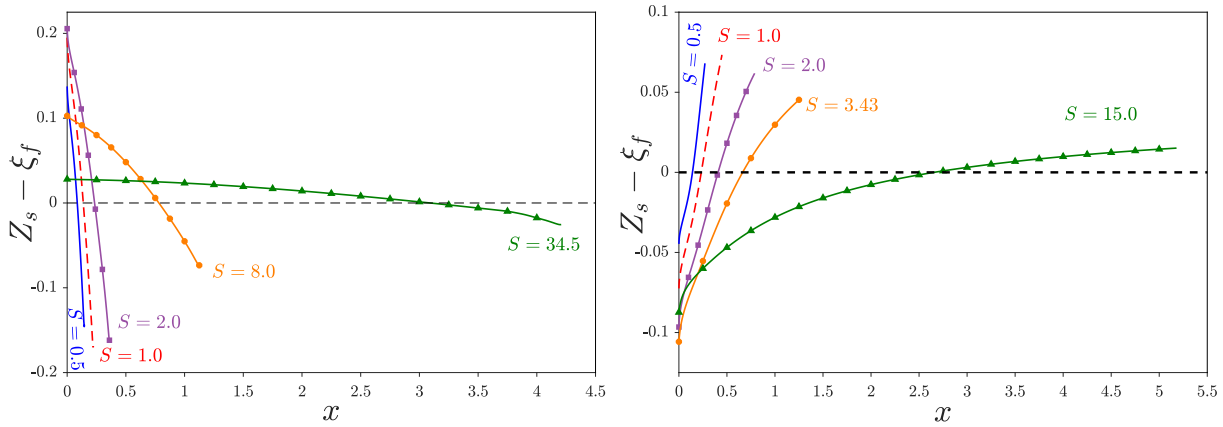

Figure 18: The dimensionless excess temperatures $Z_s - \xi_f$ for $L_{\mathrm{F}} = 0.3$ (left) and $L_{\mathrm{F}} = 2.0$ (right) with $U_0 = 1.0$

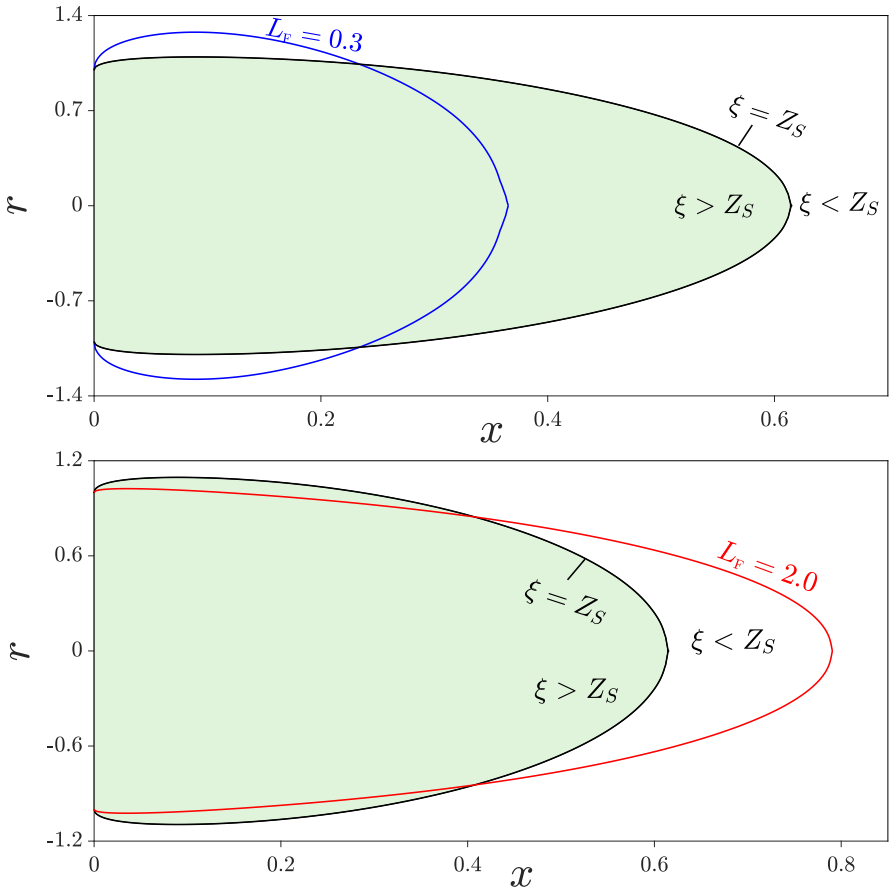

Figure 19: The flame shapes of $L_F = 0.3$ (upper plot) and $L_F = 2.0$ (lower plot) in enthalpy variable field for $S = 2$ and $U_0 = 1.0$. In the colored region $\xi > Z_s$

A.2 Planar Case

A.2.1 Governing Equations (revisited)

$$\frac{\partial U}{\partial X} + \frac{\partial V}{\partial Y} = 0 \tag{A.1}$$

$$U\frac{\partial U}{\partial X} + V\frac{\partial U}{\partial X} = Pr\frac{\partial^2 U}{\partial Y^2} \tag{A.2}$$

$$U\frac{\partial Z}{\partial X} + V\frac{\partial Z}{\partial Y} = \frac{1}{L_m}\frac{\partial^2 \tilde{Z}}{\partial Y^2} \tag{A.3}$$

$$U\frac{\partial \xi}{\partial X} + V\frac{\partial \xi}{\partial Y} = \frac{\partial^2 \xi}{\partial Y^2} \tag{A.4}$$

The system of equations must be integrated along with the initial conditions

$$X = 0 \begin{cases} |Y| \leq 1 : U = 1 \begin{cases} N: \quad Z = \tilde{Z} = \xi = 1 \\ I: \quad Z = \tilde{Z} = \xi = 0 \end{cases} \\ |Y| \geq 1 : U = U_0 \begin{cases} N: \quad Z = \tilde{Z} = \xi = 0 \\ I: \quad Z = \tilde{Z} = \xi = 1 \end{cases} \end{cases} \tag{A.5}$$

And the boundary conditions are

$$X > 0 \begin{cases} Y = 0: \quad V = \frac{\partial U}{\partial Y} = \frac{\partial Z}{\partial Y} = \frac{\partial \tilde{Z}}{\partial Y} = \frac{\partial \xi}{\partial Y} = 0 \\ |Y| = \infty : U = U_0 \begin{cases} N: \quad Z = \tilde{Z} = \xi = 0 \\ I: \quad Z = \tilde{Z} = \xi = 1 \end{cases} \end{cases} \tag{A.6}$$

N stands for normal diffusion flames and I stands for inverse diffusion flames.

A.2.2 Flame Shapes in Enthalpy Variable field

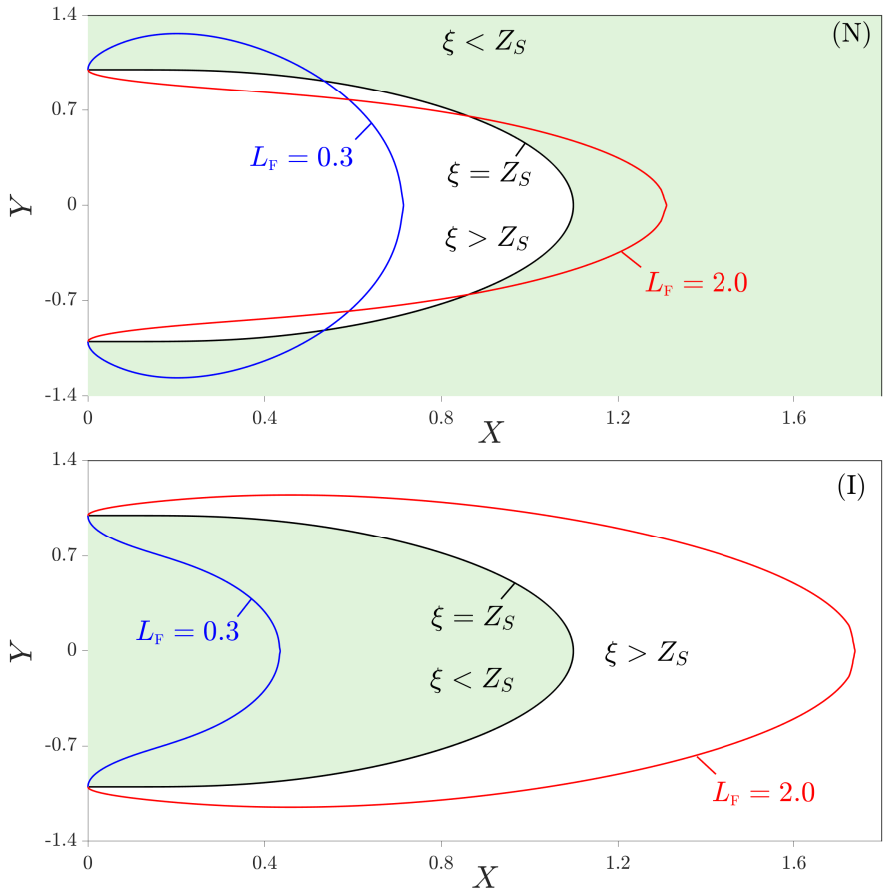

Figure 20: Isosurfaces for S = 1 and $U_0 = 1$ for normal (a) and inverse (b) configurations, including the isosurface $\xi = Z_S$ which coincides with the flame surface when $L_F = 1.0$

Fig. 20 shows the flame shapes of $L_F = 0.3$ and $L_F = 2.0$ in enthalpy variable field. In the colored (green) region is the flame temperature is superadiabatic. In Normal diffusion flame it is observed that for $L_F < 1$ the flame temperature is initially superadiabatic and downstream it becomes subadiabatic whereas $L_F > 1$ the flame temperature undergoes transition from subadiabatic to superadiabatic temperatures. Whereas for Inverse diffusion flames n such transition is observed, for Lewis number lesser than one the flame temperatures is always superadiabatic and for Lewis number greater than one the flame temperatures is always subadiabatic. This is because in inverse flames the fuel is in the outer annulus and diffuses into the flame and when is diffusivity is high all the fuel is

completely diffused into the flame and a superadiabaitc temperature is observed and as a result $L_{\text{F}} = 0.3$ has always superadiabaitc temperature and vicecersa for $L_{\text{F}} = 2.0$.

A.2.3 Effect of Lewis Number

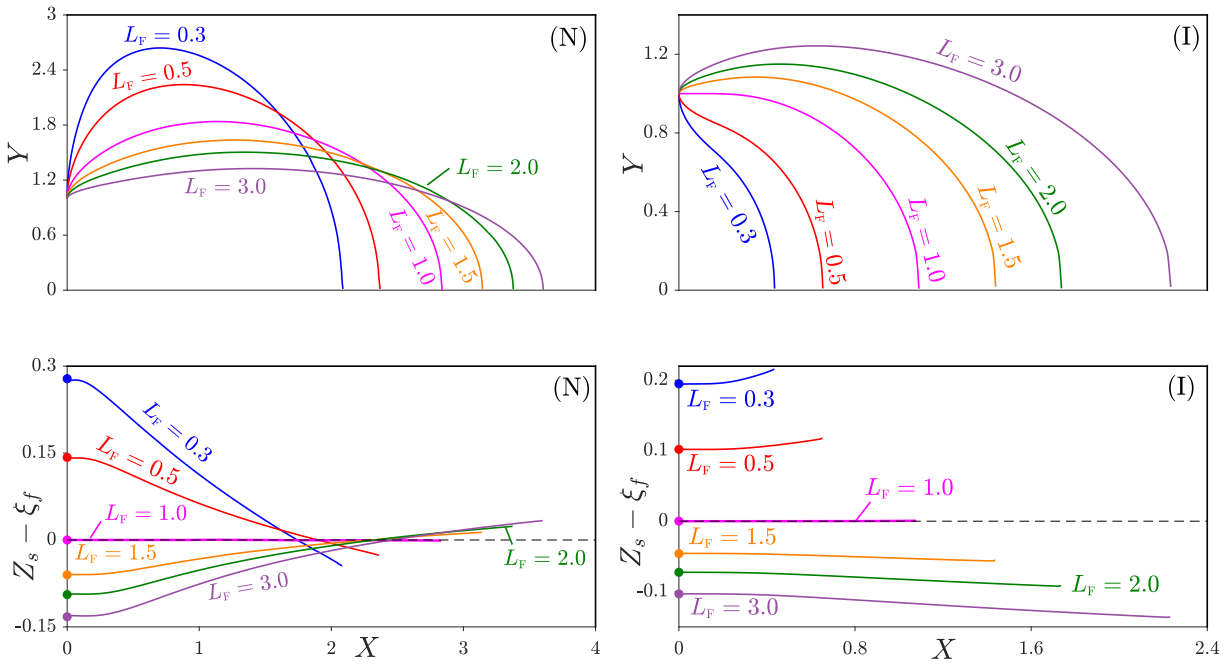

Figure 21: The variation with the fuel Lewis number L_{F} of the flame shape (upper plots) and dimensionless flame-temperature departure $Z_S - \xi_f$ (lower plots) for: Normal Diffusion flames with S = 1 and $U_0 = 0$; Inverse Diffusion flames with S = 1 and $U_0 = 1$.

Fig. 21 depicts the flame shapes and temperatures departures for various Lewis number in both the normal and inverse configurations. As Lewis number increases the flame length increases which is due to reduced mass diffusivity. The temperature departures along the flame for various Lewis numbers are shown in the lower plot of Fig. 21. The initial flame temperatures for L_{F} less than one/equal to one/greater than one are superadiabatic/adiabaitc/ subadiabaitc respectively. For $L_{\text{F}} = 1.0$, the rate of heat transfer is equal to the rate of mass transfer and as a result the flame temperature is adiabatic. Wheras for $L_{\text{F}} = 0.3$ the smaller rate of heat transfer leads to a superadiabatic flame temperature and inversely for $L_{\text{F}} > 1.0$ the larger rate of heat loss gives rise to a subadiabatic flame temperature. In normal configurations for Lewis numbers smaller than

one the flame temperatures downstream become subadiabatic, whereas for Lewis number greater than one the flame temperatures undergo transition from subadiabatic to superadiabatic. However in inverse configuration this non trivial behaviour is not observed. As expected for Lewis number equal to one $Z_s - \xi_f = 0$ along the entire flame, indicating that the flame temperature is always adiabatic i.e $T_f = T_S$. This is because for $L_{\text{F}} = 1$, $\xi_f = Z_s = 1/(S+1)$.

A.2.4 Effect of Coflow Velocity

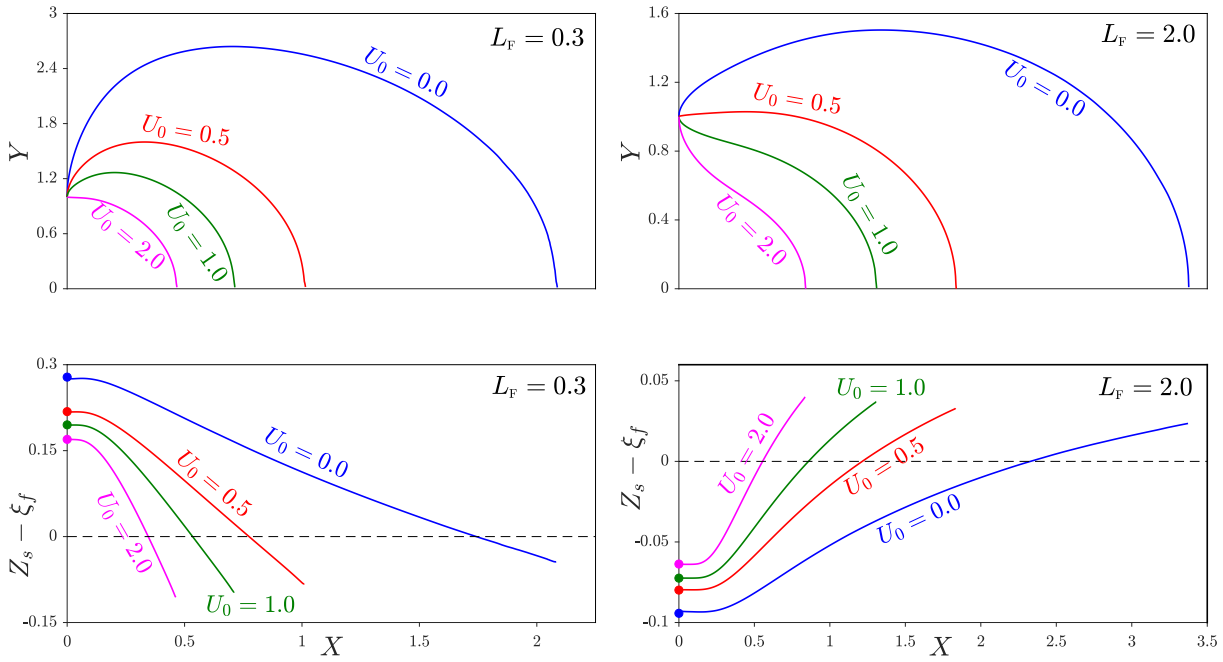

Figure 22: The variation with the Coflow Velocity U_0 of the flame shape (upper plots) and dimensionless flame-temperature departure $Z_S - \xi_f$ (lower plots) for S=1 $L_{\text{F}} = 0.3$ and $L_{\text{F}} = 2.0$.

Fig. 22 represents the flame shapes and temperatures departures for different co-flow velocities. With increase in Coflow velocity ratio the flame length decreases. For larger coflow to jet velocity ratios (U_0), the velocity of the coflowing air causes a confinement effect, which increases as the velocity of air increases. Greater confinement effect, results in a smaller flame width and flame length. In case of smaller U_0 the diffusion is slower and the fuel would advect to larger distances downstream which results in larger flame lengths.

The temperature departures in the lower plot of Fig 22 indicate that on increasing the coflow velocity the transition from super to subadiabatic flame temperature for $L_{\text{F}} = 0.3$ and sub to superadiabatic flame temperatures for $L_{\text{F}} = 2.0$ takes place earlier. Flows with higher U_0 exhibit a larger fraction of the flame that has a subadiabatic/superadiabatic flame temperature for $L_{\text{F}} = 0.3$ and $L_{\text{F}} = 2.0$ respectively. Differential diffusion effects are greater for smaller U_0 that result in a larger value of $|Z_s - \xi_f|$ near the rim of the injector ($x = 0$). As coflow velocity increases the flame moves more rapidly towards the fuel side which causes the flame temperature to undergo transition at an earlier downstream location. It is also observed that for smaller U_0 the difference in flame temperature at the injector exit and the flame tip is greater, a possible reason is due to the larger flame length.

A.2.5 Effect of Dilution

Normal Diffusion Flames

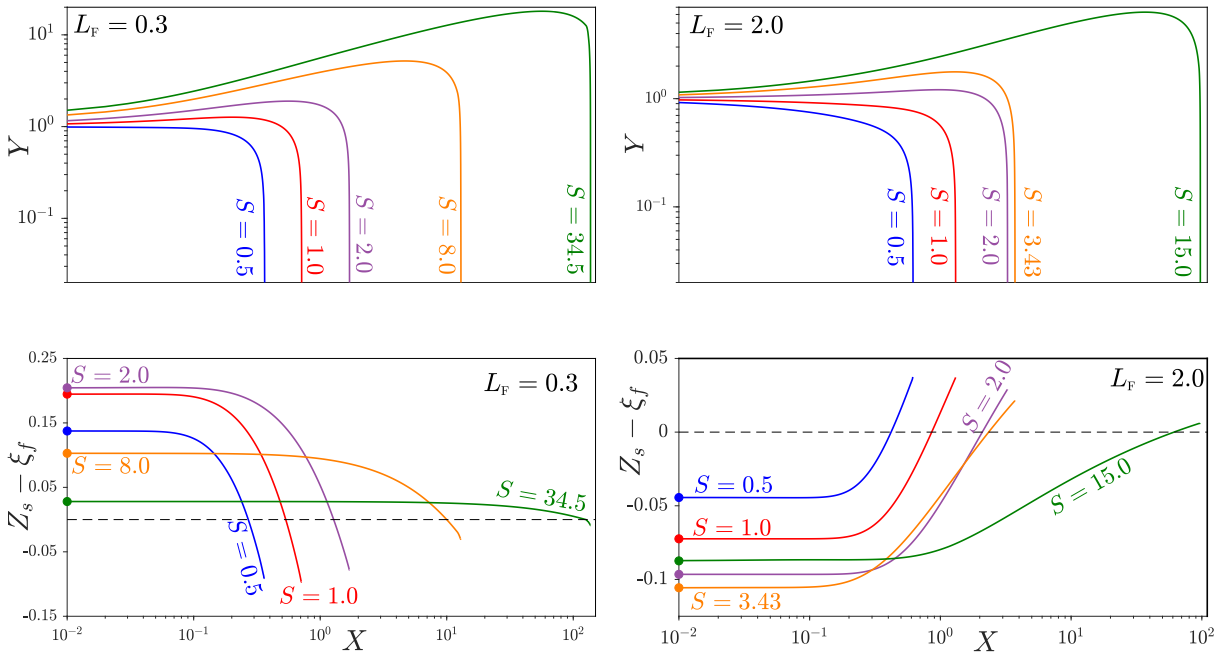

Figure 23: The variation with the dilution parameter S of the flame shape (upper plots) and dimensionless flame-temperature departure $Z_S - \xi_f$ (lower plots) for $U_0 = 1$ $L_F = 0.3$ and $L_F = 2.0$.

The flame shapes (upper plots) in Fig 23 are plotted as log (Y) vs log (X) and the dimensionless flame temperature departures are plotted as $Z_S - \xi_f$ vs log (X) . The figure shows that as the dilution increases the flame length and width decrease pertaining to the lower amount of fuel present.

The temperature departures $Z_s - \xi_f$ along the flame for $L_F = 0.3$ and $L_F = 2.0$ are shown in the lower plots Fig. 23. The magnitude of the flame temperature for $L_F = 0.3$ is maximum at the exit of the injector and decreases from there onwards. The temperature departures keep decreasing and at a certain location the magnitude of flame temperature undergoes transition from superadiabatic to subadiabatic for $L_F = 0.3$ and subadiabatic to superadiabatic for $L_F = 2.0$. This transition in flame temperatures is observed irrespective of the values of S, however as S increases the transition is delayed. This implies that for $L_F = 0.3$ ($L_F = 2.0$) a larger potion of the flame is subadiabatic (superadiabatic) for

smaller S and a smaller portion of the flame is subadiabatic (superadiabatic) for larger S. For S = 34.5 (in $L_F = 0.3$) and S=15 (in $L_F = 2.0$), subadiabatic and superadiabatic temperatures are observed only near the tip of the flame.

Inverse Diffusion Flames

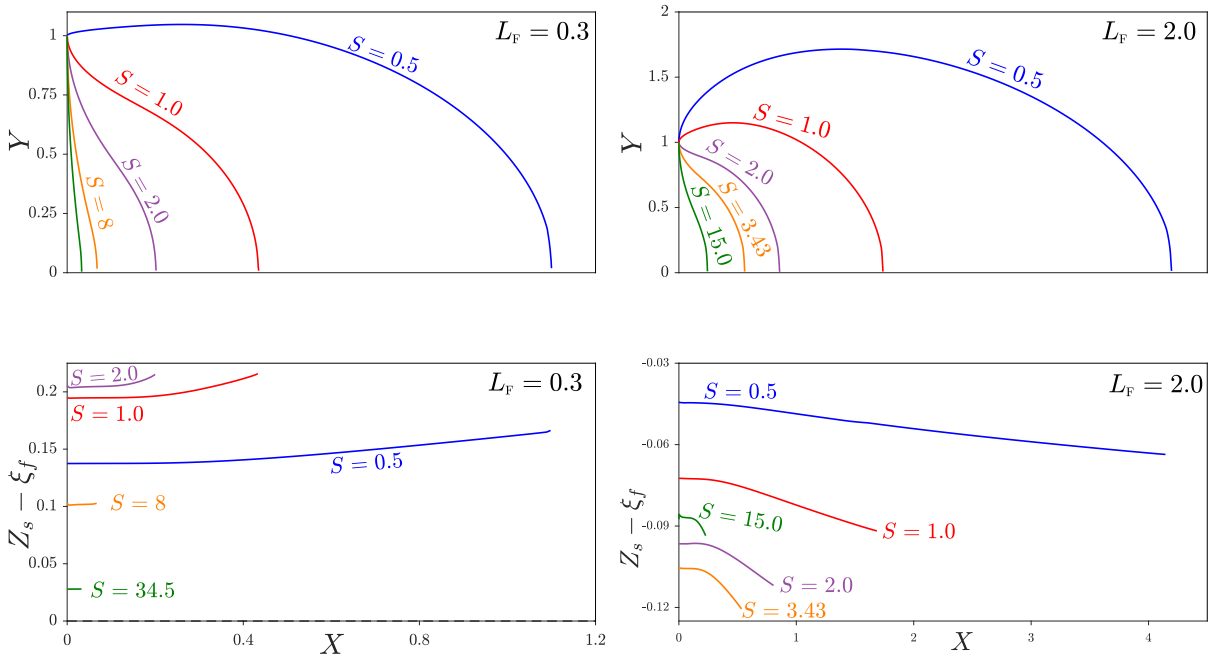

Figure 24: The variation with the dilution parameter S of the flame shape (upper plots) and dimensionless flame-temperature departure $Z_S - \xi_f$ (lower plots) for Inverse Diffusion Flames with $U_0 = 1$ (a) $L_F = 0.3$ and (b) $L_F = 2.0$.

The flame shapes(upper plots) and tmepratures departures (lower plots) for different fuel feed dilutions are shown in Fig. 24 for coflow-to-jet velocity ratio of unity i.e $U_0 = 1$. the upper plots show that as dilution increases the flame length and flame width increases. In inverse diffusion flames the oxidizer is deficient and fuel is abundant. When the dilution is low there is sufficient amount of fuel and oxidizer which would undergo combustion faster. Increase in dilution would decrease the amount of fuel, and as the deficient reactant is the oxidizer the combustion between smaller quantities of fuel and oxidise would take longer time and over a larger area. Accordingly the flame length and width would be larger for higher dilution whereas they would be smaller for lower dilution. Mathematically this

can be seen as follows, Z has to increase to the value of Z_s on the axial location and for larger dilution Z_s is larger, hence Z achieves Z_s at a later axial location. Sze et al [60] have explained the degree of entrainment as a major factor in determining the flame length and as the entrainment increases the mixing and the fuel would be burned in a premixed mode and this would result in a faster combustion and smaller flame lengths. The temperature departures indicate that the flame temperatures are always superadiabatic for $L_{\mathrm{F}} = 0.3$. The flame temperatures increase downstream and reach a maximum at the tip of the flame. Whereas for $L_{\mathrm{F}} = 2.0$ the flame temperatures are always subadiabatic and decrease along the flame and are minimum at the flame tip. This is in contrast to the nontrivial behaviour observed in normal diffusion flames. This suggests that the diffusivity of the deficient reactant in the central-jet is more important than the diffusivity of the abundant (coflow) reactant.

Bibliography

[1] SP Burke and TEW Schumann. Diffusion flames. *Industrial & Engineering Chemistry*, 20(10):998–1004, 1928.

[2] Yuenong Xu, MITCHELL D SMOOKE, PING LIN, and MARSHALL B LONG. Primitive variable modeling of multidimensional laminar flames. *Combustion science and technology*, 90(5-6):289–313, 1993.

[3] JL Ellzey, KJ Laskey, and ES Oran. A study of confined diffusion flames. *Combustion and Flame*, 84(3-4):249–264, 1991.

[4] Reginald E Mitchell, Adel F Sarofim, and LA Clomburg. Experimental and numerical investigation of confined laminar diffusion flames. *Combustion and flame*, 37:227–244, 1980.

[5] Carlos Vazquez-Espi. Analysis of axisymmetric laminar jet diffusion flames for small values of the stoichiometric mixture fraction. *Combustion science and technology*, 171(1):1–38, 2001.

[6] James A. Fay. The distributions of concentration and temperature in a laminar jet diffusion flame. *Journal of the Aeronautical Sciences*, 21(10):681–689, 1954.

[7] M Klajn and AK Oppenheim. Influence of exothermicity on the shape of a diffusion flame. In *Symposium (International) on Combustion*, volume 19, pages 223–235. Elsevier, 1982.

[8] FG Roper. The prediction of laminar jet diffusion flame sizes: Part i. theoretical model. *Combustion and Flame*, 29:219–226, 1977.

[9] D Brian Spalding. *Combustion and mass transfer: a textbook with multiple-choice exercises for engineering students*. Elsevier, 2013.

[10] S Mahalingam, JH Ferziger, and BJ Cantwell. Self-similar diffusion flame. *Combustion and Flame*, 82(2):231–234, 1990.

[11] Raymond B Edelman, Owen F Fortune, Gertrude Weilerstein, Thomas H Cochran, and John B Haggard Jr. An analytical and experimental investigation ofgravity effects upon laminar gas jet-diffusion flames. In *Symposium (International) on Combustion*, volume 14, pages 399–412. Elsevier, 1973.

[12] Raymond B Edelman and M Yousef Bahadori. Effects of buoyancy on gas-jet diffusion flames: Experiment and theory. *Acta Astronautica*, 13(11-12):681–688, 1986.

[13] M Yousef Bahadori, Raymond B Edelman, Dennis P Stocker, and Sandra L Olson. Ignition and behavior of laminar gas-jet diffusion flames in microgravity. *AIAA journal*, 28(2):236–244, 1990.

[14] PB Sunderland, BJ Mendelson, Z-G Yuan, and DL Urban. Shapes of buoyant and nonbuoyant laminar jet diffusion flames. *Combustion and Flame*, 116(3):376–386, 1999.

[15] H Sato, K Amagai, and M Arai. Diffusion flames and their flickering motions related with froude numbers under various gravity levels. *Combustion and Flame*, 123(1-2):107–118, 2000.

[16] SC Li, AS Gordon, and FA Williams. A simplified method for the computation of burke-schumann flames in infinite atmospheres. *Combustion Science and Technology*, 104(1-3):75–91, 1995.

[17] Amable Liñán, Marcos Vera, and Antonio L Sánchez. Ignition, liftoff, and extinction of gaseous diffusion flames. *Annual Review of Fluid Mechanics*, 47:293–314, 2015.

[18] A Almagro, O Flores, M Vera, AL Sanchez, and FA Williams. Effect of differential diffusion on nonpremixed-flame temperature. *Proceedings of the Combustion Institute*, in press.

[19] Y Zhang, PD Ronney, EV Roegner, and JB Greenberg. Lewis number effects on flame spreading over thin solid fuels. *Combustion and flame*, 90(1):71–83, 1992.

[20] V Katta, L Goss, and W Roquemore. Effect of nonunity lewis number and finite-rate chemistry on the dynamics of a hydrogen-air jet diffusion flame. In *31st Aerospace Sciences Meeting*, page 454, 1993.

[21] B Cuenot and T Poinsot. Asymptotic and numerical study of diffusion flames with variable lewis number and finite rate chemistry. *Combustion and flame*, 104(1-2):111–137, 1996.

[22] K Seshadri. Multistep asymptotic analyses of flame structures. In *Symposium (International) on Combustion*, volume 26, pages 831–846. Elsevier, 1996.

[23] G Balakrishnan, C Treviño, and F Mauss. The asymptotic structure of hydrogen-air diffusion flames. *Combustion and flame*, 91(3-4):246–256, 1992.

[24] Tariq Shamim. Effect of unequal fuel and oxidizer lewis numbers on flame dynamics. *International journal of thermal sciences*, 45(12):1213–1223, 2006.

[25] K Seshadri, N Peters, and FA Williams. Asymptotic analyses of stoichiometric and lean hydrogen-air flames. *Combustion and Flame*, 96(4):407–427, 1994.

[26] JS Kim and FA Williams. Extinction of diffusion flames with nonunity lewis numbers. *Journal of engineering mathematics*, 31(2-3):101–118, 1997.

[27] CK Law and SH Chung. Steady state diffusion flame structure with lewis number variations. *Combustion Science and Technology*, 29(3-6):129–145, 1982.

[28] Ruey-Hung Chen, G Bradley Mitchell, and Paul D Ronney. Diffusive-thermal instability and flame extinction in nonpremixed combustion. In *Symposium (International) on Combustion*, volume 24, pages 213–221. Elsevier, 1992.

[29] Ruey-Hung Chen*, Jose E Navedo, and Larry Chew. Effects of fuel lewis number on and damkohler number scaling of nitric oxide emission levelof burke-schumann type flames. *Combustion science and technology*, 127(1-6):293–318, 1997.

[30] Heinz Pitsch. Unsteady flamelet modeling of differential diffusion in turbulent jet diffusion flames. *Combustion and Flame*, 123(3):358–374, 2000.

[31] V Bergmann, W Meier, D Wolff, and W Stricker. Application of spontaneous raman and rayleigh scattering and 2d lif for the characterization of a turbulent ch4/h2/n2 jet diffusion flame. *Applied Physics B*, 66(4):489–502, 1998.

[32] H Pitsch and N Peters. A consistent flamelet formulation for non-premixed combustion considering differential diffusion effects. *Combustion and Flame*, 114(1-2):26–40, 1998.

[33] Eui Ju Lee, Kwang Chul Oh, and Hyun Dong Shin. Soot formation in inverse diffusion flames of diluted ethene. *Fuel*, 84(5):543–550, 2005.

[34] Ömer L Gülder and David R Snelling. Influence of nitrogen dilution and flame temperature on soot formation in diffusion flames. *Combustion and flame*, 92(1-2):115–124, 1993.

[35] KP Schug, Yaccarino Manheimer-Timnat, P Yaccarino, and I Glassman. Sooting behavior of gaseous hydrocarbon diffusion flames and the influence of additives. *Combustion Science and Technology*, 22(5-6):235–250, 1980.

[36] MD Smooke, MB Long, BC Connelly, MB Colket, and RJ Hall. Soot formation in laminar diffusion flames. *Combustion and Flame*, 143(4):613–628, 2005.

[37] A Gomez, G Sidebotham, and I Glassman. Sooting behavior in temperature-controlled laminar diffusion flames. *Combustion and flame*, 58(1):45–57, 1984.

[38] RL Axelbaum and CK Law. Soot formation and inert addition in diffusion flames. In *Symposium (International) on Combustion*, volume 23, pages 1517–1523. Elsevier, 1991.

[39] James J Feese and Stephen R Turns. Nitric oxide emissions from laminar diffusion flames: effects of air-side versus fuel-side diluent addition. *Combustion and Flame*, 113(1-2):66–78, 1998.

[40] CHARLES S McENALLY and Lisa D Pfefferle. The effect of nitrogen dilution on nonfuel hydrocarbons in laminar nonpremixed flames. *Combustion science and technology*, 151(1):133–155, 2000.

[41] Ruey-Hung Chen and James F Driscoll. Nitric oxide levels of jet diffusion flames: effects of coaxial air and other mixing parameters. In *Symposium (International) on Combustion*, volume 23, pages 281–288. Elsevier, 1991.

[42] James F Driscoll, Ruey-Hung Chen, and Youngbin Yoon. Nitric oxide levels of turbulent jet diffusion flames: effects of residence time and damkohler number. 1992.

[43] N Weiland, R-H Chen, and P Strakey. Effects of coaxial air on nitrogen-diluted hydrogen jet diffusion flame length and nox emission. *Proceedings of the Combustion Institute*, 33(2):2983–2989, 2011.

[44] Werner JA Dahm and Avrum G Mayman. Blowout limits of turbulent jet diffusion flames for arbitrary source conditions. *AIAA journal*, 28(7):1157–1162, 1990.

[45] Howard D Ross. *Microgravity combustion: fire in free fall*. Elsevier, 2001.

[46] George W Sidebotham and Irvin Glassman. Flame temperature, fuel structure, and fuel concentration effects on soot formation in inverse diffusion flames. *Combustion and flame*, 90(3-4):269–283, 1992.

[47] Christopher R Shaddix, Timothy C Williams, Linda G Blevins, and Robert W Schefer. Flame structure of steady and pulsed sooting inverse jet diffusion flames. *Proceedings of the Combustion Institute*, 30(1):1501–1508, 2005.

[48] Linda G Blevins, Robert A Fletcher, Bruce A Benner Jr, Eric B Steel, and George W Mulholland. The existence of young soot in the exhaust of inverse diffusion flames. *Proceedings of the Combustion Institute*, 29(2):2325–2333, 2002.

[49] Mark A Mikofski, Timothy C Williams, Christopher R Shaddix, and Linda G Blevins. Flame height measurement of laminar inverse diffusion flames. *Combustion and Flame*, 146(1-2):63–72, 2006.

[50] P Bhatia, VR Katta, SS Krishnan, Y Zheng, PB Sunderland, and JP Gore. Simulations of normal and inverse laminar diffusion flames under oxygen enhancement and gravity variation. *Combustion Theory and Modelling*, 16(5):774–798, 2012.

[51] SS Krishnan, JM Abshire, PB Sunderland, Z-G Yuan, and JP Gore. Analytical predictions of shapes of laminar diffusion flames in microgravity and earth gravity. *Combustion Theory and Modelling*, 12(4):605–620, 2008.

[52] Franziska Hunger, Björn Stelzner, Dimosthenis Trimis, and Christian Hasse. Flamelet-modeling of inverse rich diffusion flames. *Flow, turbulence and combustion*, 90(4):833–857, 2013.

[53] Charles K Westbrook and Frederick L Dryer. Simplified reaction mechanisms for the oxidation of hydrocarbon fuels in flames. *Combustion science and technology*, 27(1-2):31–43, 1981.

[54] FA Williams. Combustion theory 2nd, 1985.

[55] VA Shvab. Relation between the temperature and velocity fields of the flame of a gas burner. *Gos. Energ. Izd., Moscow-Leningrad*, 1948.

[56] Ya B Zeldovich. Teorii gorenia neperemeshannykh gazov. *Zhurnal Tekhnicheskoi Fiziki*, 19:1199–1210, 1949.

[57] Norbert Peters. *Turbulent combustion*. Cambridge university press, 2000.

[58] Joseph I Masters. Some applications in physics of the p function. *The Journal of chemical Physics*, 23(10):1865–1874, 1955.

[59] I Glassman and P Yaccarino. The temperature effect in sooting diffusion flames. In *Symposium (International) on Combustion*, volume 18, pages 1175–1183. Elsevier, 1981.

[60] LK Sze, CS Cheung, and CW Leung. Appearance, temperature, and nox emission of two inverse diffusion flames with different port design. *Combustion and flame*, 144(1-2):237–248, 2006.